Novel Supervisory Management Scheme of Hybrid Sun Empowered Grid-Assisted Microgrid for Rapid Electric Vehicles Charging Area

Zeeshan Ahmad Arfeen [1,2,*], Md Pauzi Abdullah [1], Usman Ullah Sheikh [1], Mehreen Kausar Azam [3], Aliyu Hamza Sule [1,4], Ghulam Fizza [1,5], Hameedah Sahib Hasan [1,6] and Muhammad Ashfaq Khan [7]

[1] School of Electrical Engineering, Universiti Teknologi Malaysia, Johor Bahru 81310, Johor, Malaysia; pauzi@fke.utm.my (M.P.A.); usman@fke.utm.my (U.U.S.); ahsulem68@yahoo.com (A.H.S.); fizashah@quest.edu.pk (G.F.); hameedah211ou@gmail.com (H.S.H.)

[2] Faculty of Engineering, The Islamia University of Bahawalpur (IUB), Bahawalpur 63100, Pakistan

[3] Institute of Business Management Sindh, College of Engineering and Sciences, Karachi 75190, Pakistan; mehreen.kausar@iobm.edu.pk

[4] Department of Electrical Engineering, Hassan Usman Katsina Polytechnic, P.M.B. 2052, Katsina 820001, Nigeria

[5] Department of Telecommunication Engineering, Quaid-e-Awam University of Engineering Science and Technology, Nawabshah 67450, Pakistan

[6] Ministry of Higher Education and Scientific Research, Al Furat Al Awsat Technical University, Najaf 54003, Iraq

[7] IoT and Big-Data Research Center, Department of Electronics Engineering, Incheon National University, Incheon 22012, Korea; ashfaq_jiskani@inu.ac.kr

* Correspondence: zeeshan.arfeen@iub.edu.pk

Abstract: The spread of electric vehicles (EV) contributes substantial stress to the present overloaded utility grid which creates new chaos for the distribution network. To relieve the grid from congestion, this paper deeply focused on the control and operation of a charging station for a PV/Battery powered workplace charging facility. This control was tested by simulating the fast charging station when connected to specified EVs and under variant solar irradiance conditions, parity states and seasonal weather. The efficacy of the proposed algorithm and experimental results are validated through simulation in Simulink/Matlab. The results showed that the electric station operated smoothly and seamlessly, which confirms the feasibility of using this supervisory strategy. The optimum cost is calculated using heuristic algorithms in compliance with the meta-heuristic barebones Harris hawk algorithm. In order to long run of charging station the sizing components of the EV station is done by meta-heuristic barebones Harris hawk optimization with profit of USD 0.0083/kWh and it is also validated by swarm based memetic grasshopper optimization algorithm (GOA) and canonical particle swarm optimization (PSO).

Keywords: electric vehicle; harris hawk optimization; energy management system; renewable sources; power electronics converter; fast charging station

1. Introduction

Rising energy demand in the transportation sector is one of the most challenging tasks to meet carbon dioxide (CO_2) reduction targets and Green House Gases emission (GHGs). Due to the sector's dependence on fossil fuel energy sources along with the monumental negative consequences in climate change, air pollution and other social impacts—electric vehicles (EVs) is a cost-effective, eco-friendly, sustainable alternative over conventional vehicles (CVs) which replace dramatically the conventional Internal Combustion Engine Vehicles (ICEV) in the present era [1]. EV exposure brings merits to power systems, such as load leveling, increasing generation capacity during high load periods, likely investment deferment, voltage regulation, spinning reserve services, reduction of oil dependence,

yielding high economic and environmental benefits. Apart from supporting the grid with active power, EVs can enhance the power quality by supplying power to the grid especially at peak load. The total amount of emissions produced by an electric vehicle over its entire life cycle, which includes both the energy input and the materials utilized to power the vehicle from tank to wheel. The direct tailpipe emissions which are termed as well to wheels is far less than ICEV [2,3]. As EV is empowered by batteries there is remarkable research in battery technology. Gaston Planté was the first French physicist who invented the lead-acid battery in 1859. This type of battery was developed as the first rechargeable electric battery marketed for commercial use and it is widely used in automobiles [4]. From that time battery chemistry is improving day by day and now Lead-acid, Lithium-ion battery, sodium nickel chloride (NaNiCl2) battery also known as ZEBRA, the name originated from the Zeolite Battery Research Africa Project (ZEBRA) group in South Africa, metal air batteries, sodium beta batteries are well competing in the vehicle market [5]. Figure 1 gives a clear comparison between these internal combustion and electric powered vehicles [6].
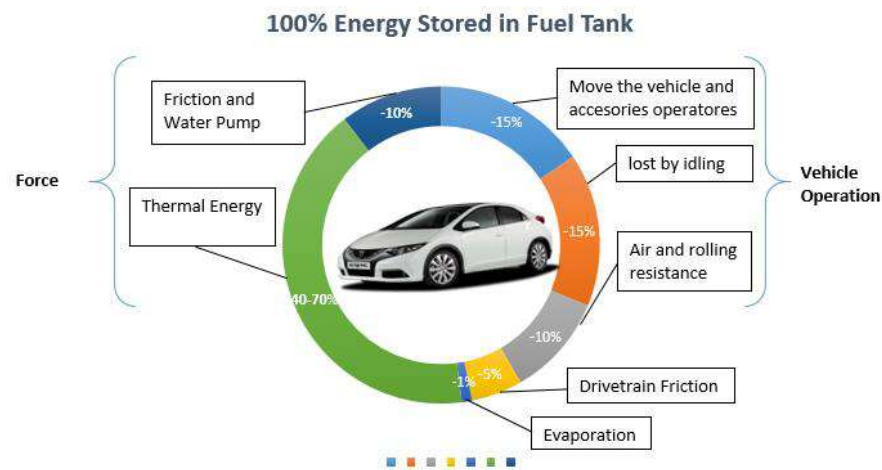

Figure 1. Comparison pattern ICEV versus EV.

Integrating an EV fast-charging station into a weak AC grid can result in protection system issues and steady-state voltage/frequency regulation problems. Moreover, the intermittent and fast load changes associated with the fast-charging of EVs give rise to dynamic voltage regulation problems [7]. In paper [8] the authors developed green building management scheme (GBMS) using renewables with the long and short term storage devices. The simulation shows that control schemes of GBMS is tested superbly. In another paper [9] driving pattern of commercially vehicle fleet and integration of Battery Electric Vehicles (BEV) is computed. Lessening of GHG and gross price of possessions also worked out. An algorithm is based on mixed integer linear program (MILP), utilizing MATLAB incorporated with solver was developed that combines variable charging set ups, the mobility contour and variant vehicle classes, to organize an optimized norm for organization. Similarly in a survey paper [10], the authors discusses various charging tactics of EVs. The authors also debates about intricacy; socio-economics and line losses on the mainstream; competence to give ancillary services; operation prospects (charging duration) and direct effect on the vehicles, public grid and the atmosphere. In paper [11] authors introduced the new green building network which permits the proficiency of model-based expansion for energy management algorithms in smart buildings or predictive renewables strategies for hybrid vehicles with electromotive drive train. In the paper [12], EV charging station is used using renewables which smoothen the excess power, to enhance features of the home-grid interface using BMS (Battery Management System) and power inverter. In the paper [13], the integration of BEV in the commercial company is investigated with the potential to raise profitability while charging. In the paper [14] the driving pattern of industrial fleet is rigorously evaluated and possibility of maximum BEV in compliance

with smart charging scheme. Lessening of nitrogen gases and gross ownership of vehicles also discussed. In another research [15] the authors simulated the GPS installed taxies with four different models of PHEV. They developed data set comprising SoC traces, load charge, charging time and for V2G applications. The authors in [16] proposed a parking lot management scheme (PLMS) with recharging management scheme (RMS) for rescheduling of EV empower with solar power with the aim of reducing the power taken from the mains during high rise pricing duration.

In the studied paper the heuristic supervisory rule-based energy management scheme is applied to manage the electric vehicle loads from stochastic PV generators in addition to battery storage buffer for seamless daylight charging operation with a facility at a lower price as compared to direct charging from the grid. The process runs in such a way that no interruption in charging and lesser impact on the grid load occurs while the electric station does not fall in the deficit. The one-line diagram of the precedence allocation of the vehicle charging is schematically drawn in Figure 2 [17]. The proposed charging station can mitigate the grid voltage regulation problem by limiting the station's imported power to a pre-specified limit and confine the EV-charging dynamics within the station. This requires a Supervisory Controller (SC) that controls the battery energy storage system (BESS) charging/discharging by coordinating the operation of controllable units within the station.
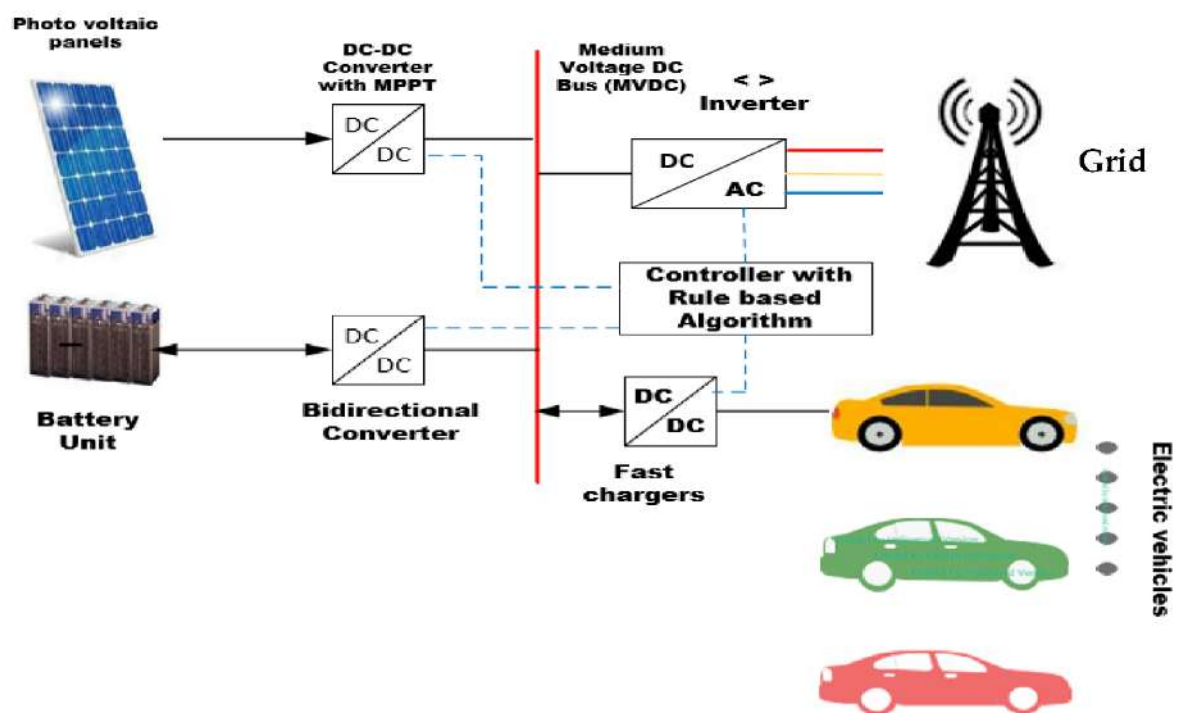
Figure 2. One line diagram of energy management of charging station. Reprinted with permission from ref. [17]. Copyright IEEE Xplore.

This paper presents and develops a supervisory controller for the battery-enabled DC fast charging station based on the Supervisory Control Theory (SCT) of discrete event systems. The proposed SCT is (i) based on a rigorous mathematical process, (ii) modular, (iii) scalable, and (iv) logically optimized, i.e., guarantees non-blocking and minimally restrictive properties concerning the discrete plant behavior and is subject to the supervisory control specifications. The supervisory control also can use a Finite State Machine (FSM) for the implementation of complex supervisory control logics which is transparent and readily implementable on industrial controllers.

1.1. Work on Smart Fast Charging EV

Despite the environmental and economic benefits, EVs adverse the power utility if smart charging techniques are not utilized. Due to the unpredictability of both load and power generation from renewable energy sources, power imbalances occur between the generation and the load. To maximize the usage of RES and limit the impact of the EVs' charging from the utility AC grid, a smart power-flow charging algorithm necessitates and rules should be designed [18].

Papers [19,20], introduced a smart real-time Fuzzy Logic controller (FLC) to minimize the influence of EVs on the public grids and lessens the vehicle charging cost. The same author [20], developed a real-time algorithm for a grid-oriented charging carport in a commercial workspace. The algorithm targets to minimize the daily overall price of charging of the EVs, smoothing the effect of the electric station on the mains, and participating to shave the peak load curve. The charging rate (C) is assigned depending upon charging priority levels. However, the paper is good to implement if energy storage banks are used for standby power for balancing the intermittency issues of photovoltaic. Horizon Markov finding method (MFM) is selected in the paper [21] for the efficient control of a solar-oriented EV charging station. The model features the vehicle to grid (V2G) application to offer ancillary services and facilitates dynamic electric cost depends on the time of use (ToU) tariff and takes into consideration the ambiguity of vehicle owners' parking behaviors. Similarly Tianxiang Jiang [22], introduced a smart EV charging controller having a classical charger which has pre-set recharging current profile, irrespective of the battery state health. Rama et al. [23], directly controlled the EVs charging by regulating the power converter switches of DC rapid electric station with a novel FC/reduced FC (fixed current) approach. Another in [24], the paper proposed a control scheme for a station composed of a photovoltaic (PV) array, energy storage unit and corresponding converters. The practical feasibility of a control strategy was previously tested by simulations in [25]. The strategy proposed was based on four different operation modes: grid-connected rectification, PV charging and grid-connected rectification, PV charging and grid-connected inversion. The switching between the modes of operation occurred due to the change in the voltage level at the DC link that varied with the change in the irradiation on the PV plates. In another recent study [23], the authors developed the model of a DC fast charging station of 50 kW. The simulations to evaluate the fast charge control, DC-link voltage control and the reactive power compensation control were carried out by using PSCAD/EMTDC software [26]. In Ref. [27], a small-sized superconducting magnetic energy storage (SMES) was proposed as a power stabilizer during transient operation to maintain the DC bus voltage. The proposed ESS was compared with the other quick response energy storage technologies like: super-capacitors and flywheels. The regulation strategy was verified by simulations in MATLAB/Simulink but modelling of the elements and power electronic interfaces needed to implement the station was not discussed in this reference. The schematic diagram of SEMS storage is portrayed in Figure 3. In paper [28], the authors proposed an artificial neural network (ANN) and adaptive neuro-fuzzy inference system (ANFIS) controller, due to the limited functions of the classical EV charging controller. This adaptive controller has a concurrent smart control to meet customer's demands, provide an active power process, and extend vehicle battery lifetime. Even though the paper has many settling issues each problem in a broadband prospect. Oliveira et al. [29], the authors besides transferring energy to the load during the recharging period, also install capacitor banks to lessen electrical losses and recuperate voltage states during vehicle charging with the help of Artificial Immune Systems (AISs). In Ref. [30] defines the control techniques based on smart communications with or without control scheme, subjugated with multi renewable sources offering electrical power. In the paper [31], a resilient residential energy management scheme is devised which is capable of monitor and control of domestic loads. The scheme is dependent on an enhanced, competitive binary grey wolf accretive satisfaction algorithm, which is developed on the hypotheses that time-varying priorities are quantifiable in terms of time and device-dependent features.
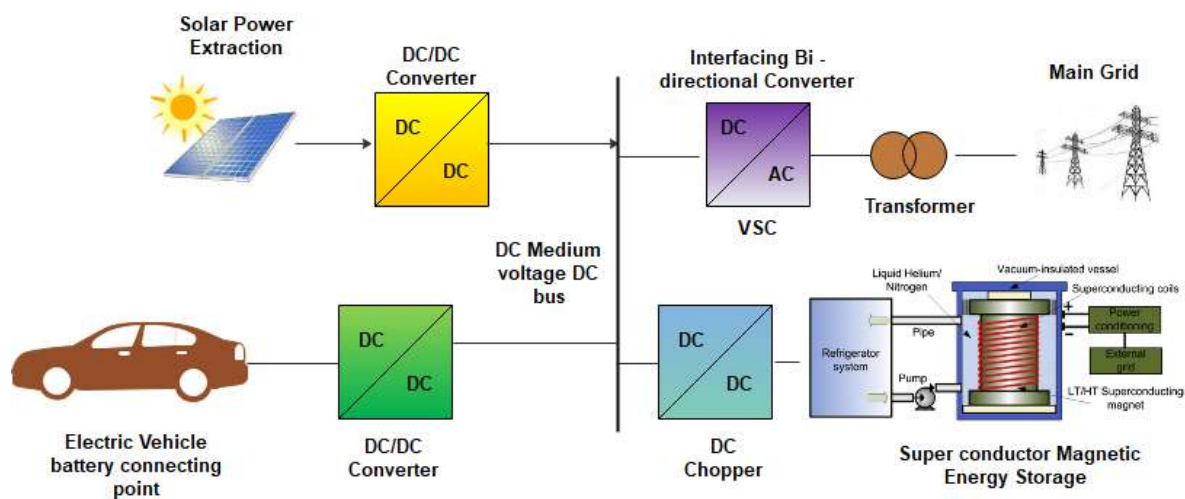
Figure 3. EVCS with hybrid PV/ESS and SMES with a grid.

For optimal sizing papers, several papers are written on the subject. In the paper [32] for system sizing and selecting renewable units (wind/PV/diesel), an energy deterministic algorithm is used for an autonomous system to lessen the gross price of the network while assuring the satisfaction of the load demand. In the paper [33], an effective price response scheme for EV customers is given which facilitates EV diurnal carport station integrated with solar arrays. For this strategy, a biased PSO applied for the time of use (TOU) tariffs and peak-flat-valley time-division recharging service is applied.

1.2. Contribution

Previously the configuring of the electric station and the design of energy management schemes (EMSs) have not been deeply earthed specifically, in the case of stations empowered by RES. The paper contributes in the following actions;

- Seamless daylight electric charging is proposed for the employees, staff, and students which facilitated the owners with less cost.
- By utilizing a shrewd energy management scheme the impact on the mains is very less and take advantage of the grid whenever the price of the grid decreases.
- Optimum sizing of charging station components is done by artificial indigence, meta-heuristic swarm-based algorithm for an optimum number of battery units and PV panels.
- It is also validated with memetic grasshopper optimization (GOA) and canonical particle swarm optimization (PSO).

1.3. Organization of Paper

The organization of the paper is framed as: architecture of EV fast-charging station, mathematical modeling of fast charging station components in Section 2. Section 3 covers the supervisory rule-based energy management methodology of the understudied work, possible number of modes, big scenarios with a flow chart. Section 4 slots the confab and discussion with the resiliency of the rule algorithm under different situations. Section 5 ends with the concluding remarks and futuristic approach.

2. Mathematical Modeling of EV/DC Fast Charging Station

The studied system is composed of fast chargers, PV system, Li-ion ESS, and the grid connection. All of the elements are tied to a medium voltage DC bus (MVDC) common bus via their corresponding power converter, which ensures the charge of a fleet of EVs with a precise power supply. Additionally, it controls the power balance between the sources and the DC bus. Furthermore, the grid connection consists of a bi-directional DC/AC converter and a transformer. Concerning the DC bus, its application is first reported in

the design of shipping power [34]. DC architecture advantage is an easy and efficient way, both for stationary storage systems and RESs. The use of proper unidirectional and bidirectional DC/DC power converters makes it comfortable to integrate and smart energy exchange among different energy sources, electric loads and storage systems. This DC configuration presents the key characteristic of avoiding any kind of AC conversion stage within the charging station, increasing as a consequence the whole energy conversion efficiency. The implementation of the DC bus, in general, leads to higher efficiency and greater system reliability. As obvious, it reduces the necessary power conversion stages. This in return, reduces the loss in the power conversion process and simplifies the control algorithm [35–37]. Furthermore, the DC bus provides seamless power management and increases the prospect of integrating other types of renewable power sources.

The voltage source converter (VSC) control the inverter-based insulated gate bipolar transistor (IGBTs) which sustains the DC bus voltage at medium voltage V_{DC}, the transient state fluctuations are minimized with an adequate level of efficiency.

2.1. Modelling of Photovoltaic Generator

PV power generation has numerous advantages if compared with other green sources; such as installation flexibility with minimum maintenance. PV integration in the distribution system is widely accepted due to universal sunlight availability, high modularity, easy maintainability, long life cycle and mobility, short time for design, incurring no fuel operation cost, environment-friendly, installation and start-up, and the ability for off-grid application [38]. PV array installation is easy and the continuous price reduction of PV modules makes it more attractive. Hence, PV array-based EV battery charging is adopted by many EV users [39]. Despite clear advantages, solar PV is un-dis patchable with fluctuating power output which results in voltage variation, degraded protection, leakage power flow, non-availability during the night and increased fault level [40,41].

An equivalent circuit of a solar cell consist of a single diode model is selected for this configuration. It consists of a current source in parallel with a diode with shunt and series resistance. An equivalent model of tandem solar cells is displayed in Figure 4 [17].
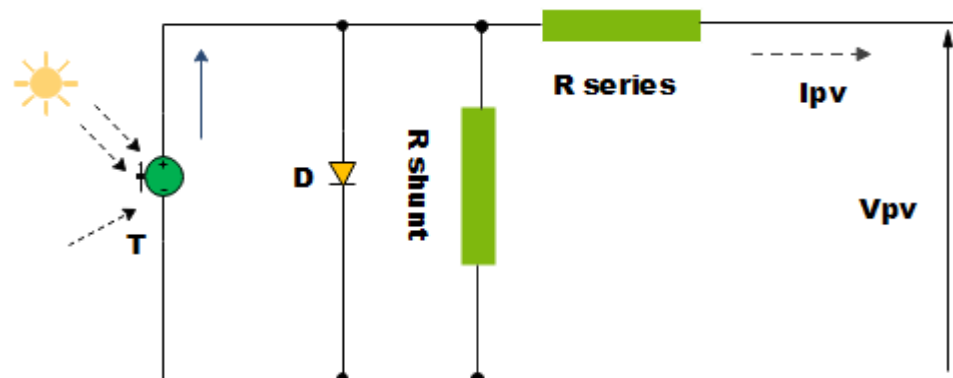

Figure 4. Equivalent model of PV cell. Reprinted with permission from ref. [17]. Copyright 2021 from IEEE.

The PV output is calculated with the help of a single diode model. The output current of PV primarily depends on temperature (T) and solar irradiance intensity (G). The output current of PV, i.e., I_{pv}, is given in;

$$I_{pv} = I_{ph} + I_{sat} \left(e^{q \left(\frac{V + I_{pv} * R_s}{NKT_{PV}} \right)} \right) - \frac{V + I_{pv} * R_s}{R_{sh}} \tag{1}$$

$$I_{ph} = I_{pho}(1 + k_0(T - 300)) \tag{2}$$

$$I_{sat} = k_1 T^3 e^{\frac{-qV_g}{KT}} \tag{3}$$

I_{ph} − solar induced current
I_{pho} − solar induced current at 300 °C
I_{sat} − saturation current of the diode
V_g − voltage applied to the terminals of diode
k_0, k_1 − constants depend on the value of PV system
T_{PV} − operating temperature
N − diode quality factor

$$V = \frac{((a \times K \times t))}{q} \tag{4}$$

V = thermal voltage
q = electron elementary charge (1.602×10^{-19} C)
a = ideality factor ($1 < a < 2$)
k = Boltzmann constant (1.381×10^{-23} J/K)
R_s *and* R_p are series and shunt resistances, respectively.

The output power of the PV generator at time step t is calculated by the following equation [42];

$$P_{pv}(t) = N_{pv} \times \eta_{pv} \times A_{pv} \times \frac{G_i(t)}{1000} \tag{5}$$

where η_{pv} is the efficiency of the PV panels, A_{pv} is the area of each PV panel in m^2, $G_i(t)$ is the aggregate solar irradiation incident on the tilted PV panels in W/m^2 at time step t, and N_{PV} is the optimum number of panels that are determined at each iteration of the optimal sizing procedure. The most crucial feature of the MPPT is its ability to track the MPP as quickly and efficiently as possible. These can be configured using a fixed or adaptive time step. The algorithm used for maximum tacking is used Perturb and Observe method. The yearly temperature variations and solar insolation are delineated in Figures 5 and 6.
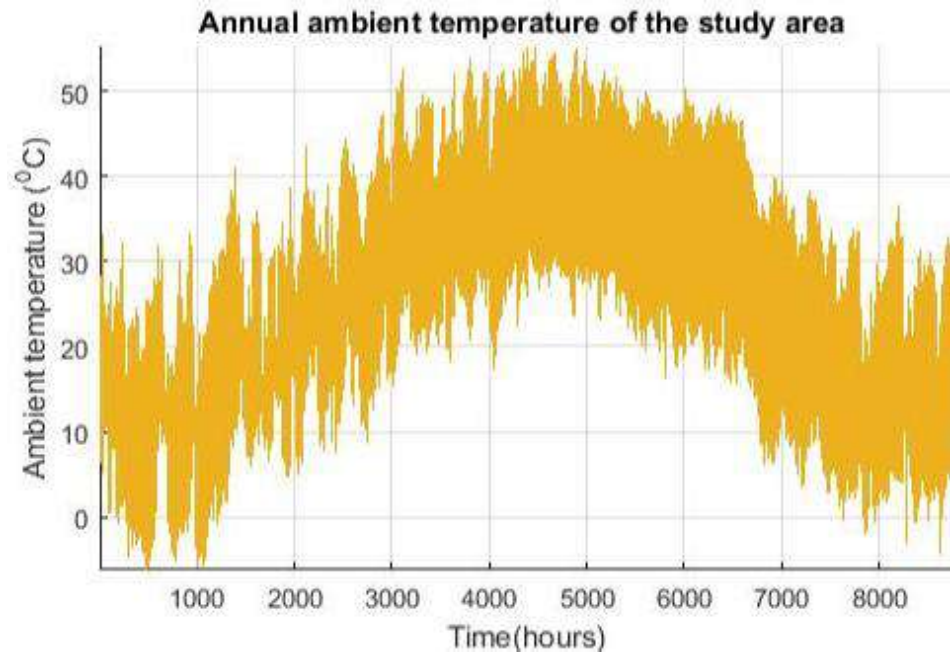

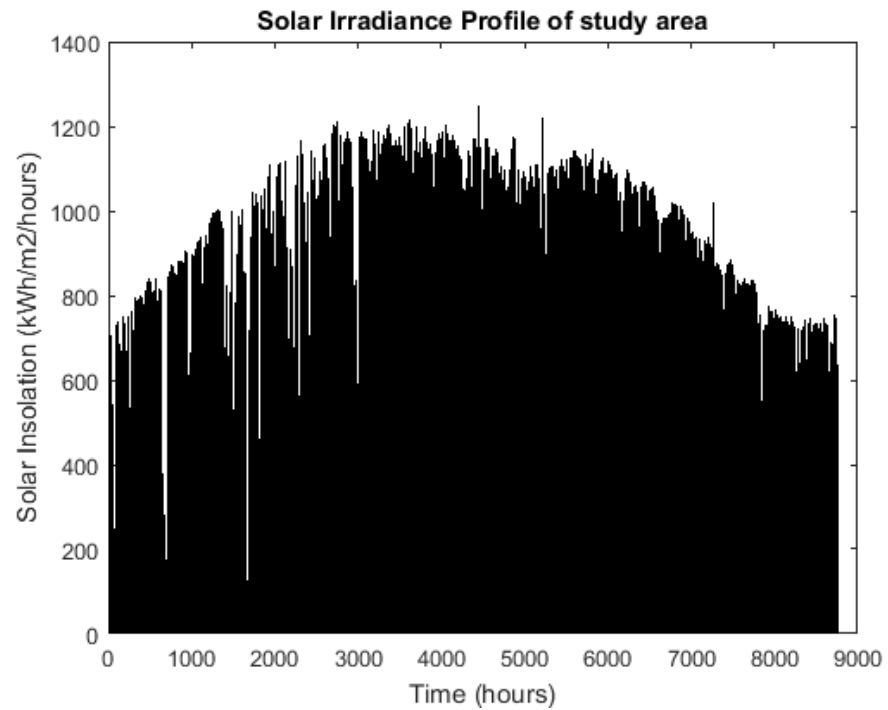**Figure 5.** Temperature variations of a studied area over a year.

Figure 6. Irradiance horizon of a photovoltaic cell for a year.

2.2. Modelling of Energy Storage Stacks

Charging stations with stationary energy storage stacks are intrinsically capable of providing services to distribution utilities. It plays a fundamental role in the integration of EV fast electric stations as they act as backup systems and ease fast charging under adverse generation conditions. The underneath equation is used to model the state charge (SOC) of the battery banks at each time step t [43]

$$E_b = E_b(t-1) + P_{ch}(t) \times \eta_{ch} \times \Delta t - \left(\frac{P_{dch}(t)}{\eta_{dch}} \right) \times \Delta t \tag{6}$$

where $P_{ch}(t)$ is the delivered electricity from the renewable energy sources to the battery packs, $P_{dch}(t)$ is the energy delivered from the battery modules to the inverter, η_{ch} and η_{dch} are the charging and discharging efficiencies of the battery bank respectively.

Initially, the ESS was reflected to be 30% charged with the rated capacity. When $P_{bat}(t) < 0$, it shows a power generation deficit. $P_{bat}(t) > 0$ shows the indicator of battery power generation having surpassed energy demand. Charging of battery occurs when $SOC > SOC_{min}$ or $P_{pv} > P_d$ and therefore the charge state of the battery is represented below;

$$SOC(t) = SOC(t-1) * (1 - \tau) + \left(P_{pv} - \frac{P_d}{\eta_{inv}} \right) \times \eta_{bat} \tag{7}$$

Likewise, if there is a power demand and the battery storage system can discharge (i.e., $SOC > SOC_{min}$), to meet the demand of energy than it can be represented by the equation:

$$SOC(t) = SOC(t-1) * (1 - \tau) + \left(\frac{P_d}{\eta_{inv}} - P_{pv} \right) \times \eta_{bat} \tag{8}$$

where,

$$\tau = Battery\ self\ discharge\ rate;\ \eta_{bat} = Battery\ efficiency;\ P_d = Power\ demand$$

The power required by the ESS (i.e., *Red_ESS_Pwr*) is outlined as a least power value that rises its level of charge from the initial to maximum value of SOC (i.e., SOCM) in definite time step (Δt) as defined by;

$$Red\_ESS\_Pwr(t) = \frac{(SOCM - SOC(t) \times N_{bat} \times Q_{bat}}{\Delta t} \tag{9}$$

Similarly, the power obtainable with ESS (i.e., *Avl_ESS_Pwr*) is stated as an extreme power that can be provided seamlessly by ESS for the given time step (Δt) before the state of charge reaches its lower bound (called *SOCL*) defined by:

$$Avl\_ESS\_Pwr(t) = \frac{(SOC(t) - SOCL) \times N_{bat} \times Q_{bat}}{\Delta t} \tag{10}$$

2.3. DC Fast Charger

The primary function of a DC fast charger module is to match the DC bus voltage to the EV battery so that the charging can be effectively controlled. The bidirectional topology is used because of the future expectation that the EV charger will include the Vehicle 2 grid (V2G) function. The DC charger module comprises of parallel off-board converters that interface the internal bus voltage to the output charging bus. The output bus voltage is then regulated according to the EV battery pack terminal voltage to charge or discharge the battery pack. In the MVDC model, the EV charging station employs level 3 DC fast chargers, which have the capability of charging within 30 min [44]. Figure 7 shows the charging topology of the constant current constant voltage (CC/CV) charging strategy [23].
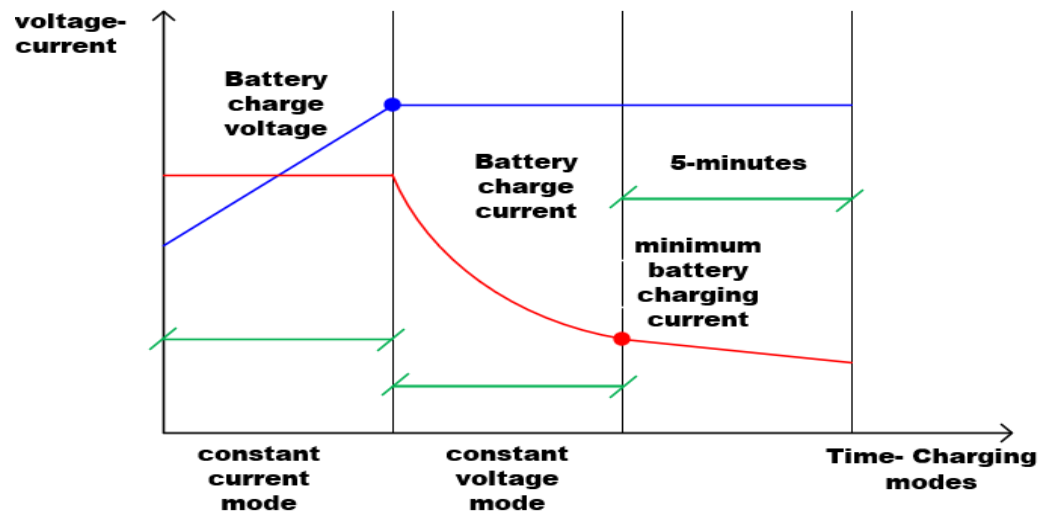

Figure 7. Processing of *v* and *i* during the charging process. Adapted from ref. [23]."

3. Research Methodology

The sizing of the electric station by optimum values of solar modules and battery units, a rule-based energy management algorithm (REMA) is understudied in the paper. It is envisaged that the proposed REMA is embedded in the centralized controller to automate control of the system. The framework of the proposed scheme is depicted in Figure 8.
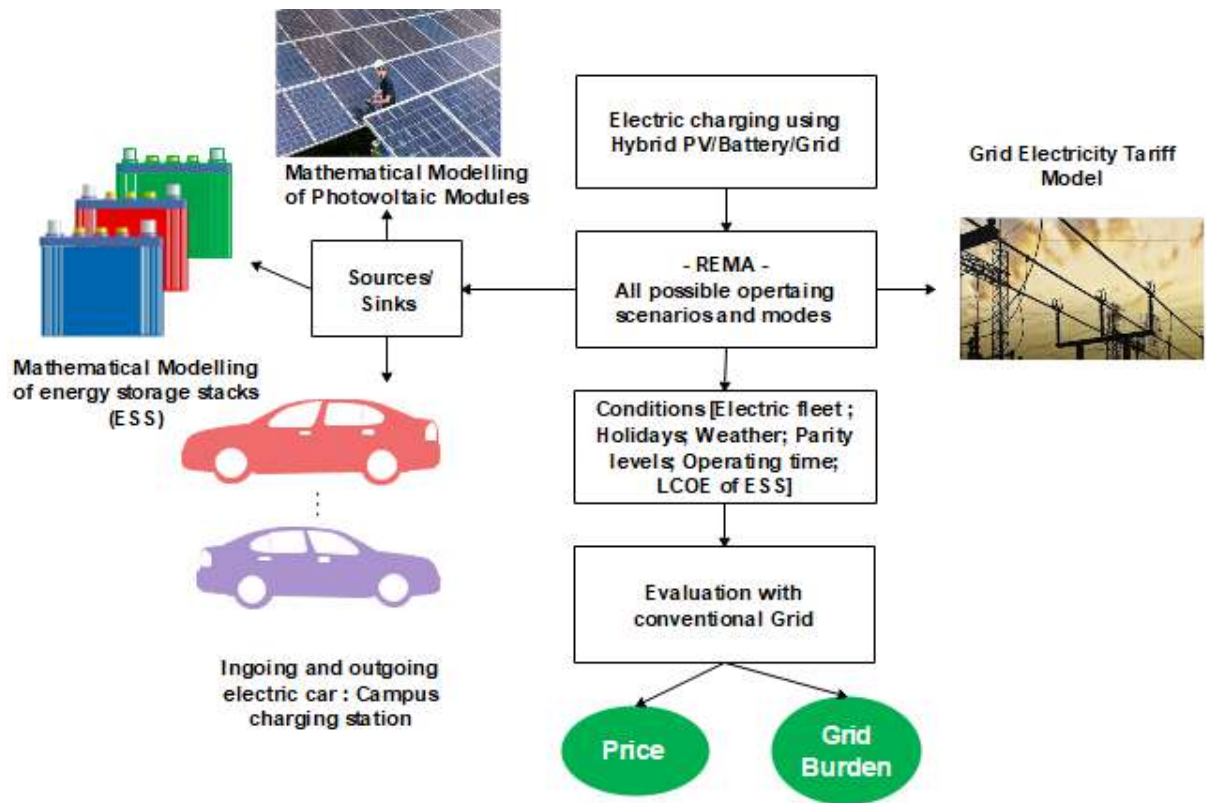
Figure 8. Framework of research methodology.

The parameters used for the simulation of the proposed restructured allocation energy management enlisted in Table 1.

Table 1. Parameters used in the research.

Sr. No	Design Parameters	Report
1	Grid Electricity Cost (*GD_Co*)	Hypothetical value for par and below parity
2	Rated capacity of PV modules	325 kilowatts
3	Polycrystalline PV panels	Canadian Solar CS6U-325P
4	Charging Cost of EV (*Chg_Co*)	(*PV_Co -1.0*) = 16 cents/kWhr
5	Levelized cost of electricity (LCOE) of PV panels (*PV_Co*)	17 cents/kWhr [45]
6	LCOE of ESS (*ESS_Co*)	15.2 cents/kWhr [46]
7	Minimum number of ESS batteries N_{bat}	Find by HHO, GWO, PSO
8	Minimum number of PV modules N_{pv}	Find by HHO, GWO, PSO
9	Maximum number of EV Fleets	150/day
10	Location of meteorological data	California NREL
11	EV power Demand (*EV_Dmd*)	Using model given in [47]
12	PV Power (*PV_Pwr*)	By means of a single diode model with meteorological records extracted from [48]
13	At Parity state (PS)	*Mean GD_Co* = LCOE of PV
14	Below parity @ (0.83PS)	*Mean GD_Co* = 1.2 * LCOE of PV
15	Below parity @ (0.33PS)	*Mean GD_Co* = 3 * LCOE of PV
16	Grid electricity cost (*GD_Co*)	Variation depend upon load
17	SOC of (*ESS_Pwr*)	Mathematical model from [49]

3.1. Modeling of Electric Vehicle Power Demand

Power required by the EV (named as *EV_Dmd*) is modelled from [50]. The request for the power charging of a single-vehicle at a particular duration *t* can be estimated as;

$$P_{EV,t} = P_{EV,req} \times s_t \times w_t \times h_t \tag{11}$$

where $P_{EV,req}$ is the power anticipated by the battery for rising the *SOC* from the initial value (SOC_0) at the time of plugin to the final value (SOC_{max}) in an interval period Δt. s_t is the signal for monitoring *SOC* of the vehicle battery. The w_t *and* h_t represent the campus working days with campus working hours, respectively.

For random *EV_Dmd*, the displacement covered by the vehicle by the last charging (T_d) is generated randomly between 1 mile to the extreme EV journey (R_t). Based on journey distance (T_r), the gross energy accumulated by EV during the last journey range (E_R) is computed as;

$$E_R = T_d \times E_m \tag{12}$$

where E_m is energy utilization/mile for the given EV. From E_m and the gross battery capacity (Q_{bat}) of the EV, SOC_0 is computed as;

$$SOC_0 = 1 - \frac{E_R}{Q_{bat}} \tag{13}$$

Furthermore, at the start of the plugin, the parameter SOC_0 applied to assess the power desired by the unit vehicle ($P_{EV,req}$) as given as:

$$P_{EV,req} = \frac{(SOC_{max} - SOC_0) \times Q_{bat}}{\Delta t} \tag{14}$$

By inserting $P_{EV,req}$ and decision signals s_t, w_t, *and* h_t in base equation, the power demand of unit vehicle at time *t*, $P_{EV,t}$ is computed. However, for a fleet of vehicles, $P_{EV,t}$ is summed to achieve the accumulated *EV_Dmd*.

$$EV\_Dmd, t = \begin{cases} \sum_{n=1}^{N} P_{EV,t}^n \text{where } t \text{ is the campus hours} \\ 0, \text{ else} \end{cases} \tag{15}$$

where *N* is the maximum number of e-vehicles arrived at the station and $P_{EV,t}^n$ is the required power by the *nth* car at a given time *t*. Probability distribution was drawn based on an appropriately ample number of autonomous random variables i.e., inbound and outbound EV at the charging facility each with the set population mean (μ) and variance (σ). Cascading the probability distribution function (pdf) of arrival and departure time (A_t *and* D_t), the allied pdf of $D_t - A_t$ can originate, which is usually parking time. The pdf of the common parking staying time portrayed in Figure 9 as defined in [19].
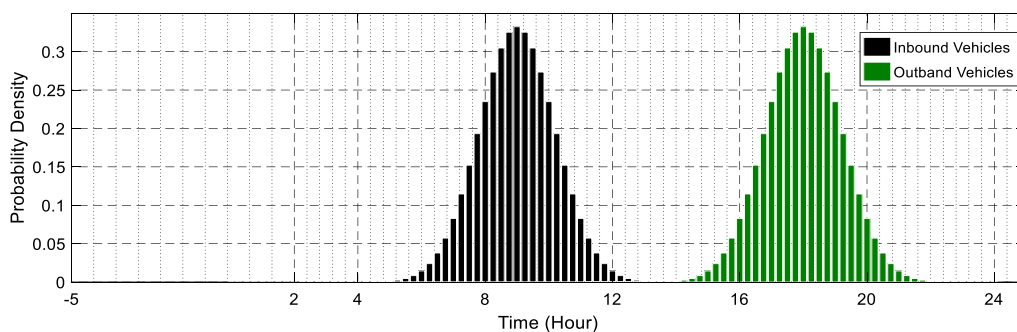
Figure 9. Hourly Probability Density Function of a fleet of vehicles. Reprinted with permission from ref. [19]. Copyright from IEEE.

The flow chart of the power-desired model for a unit vehicle is marked in Figure 10.
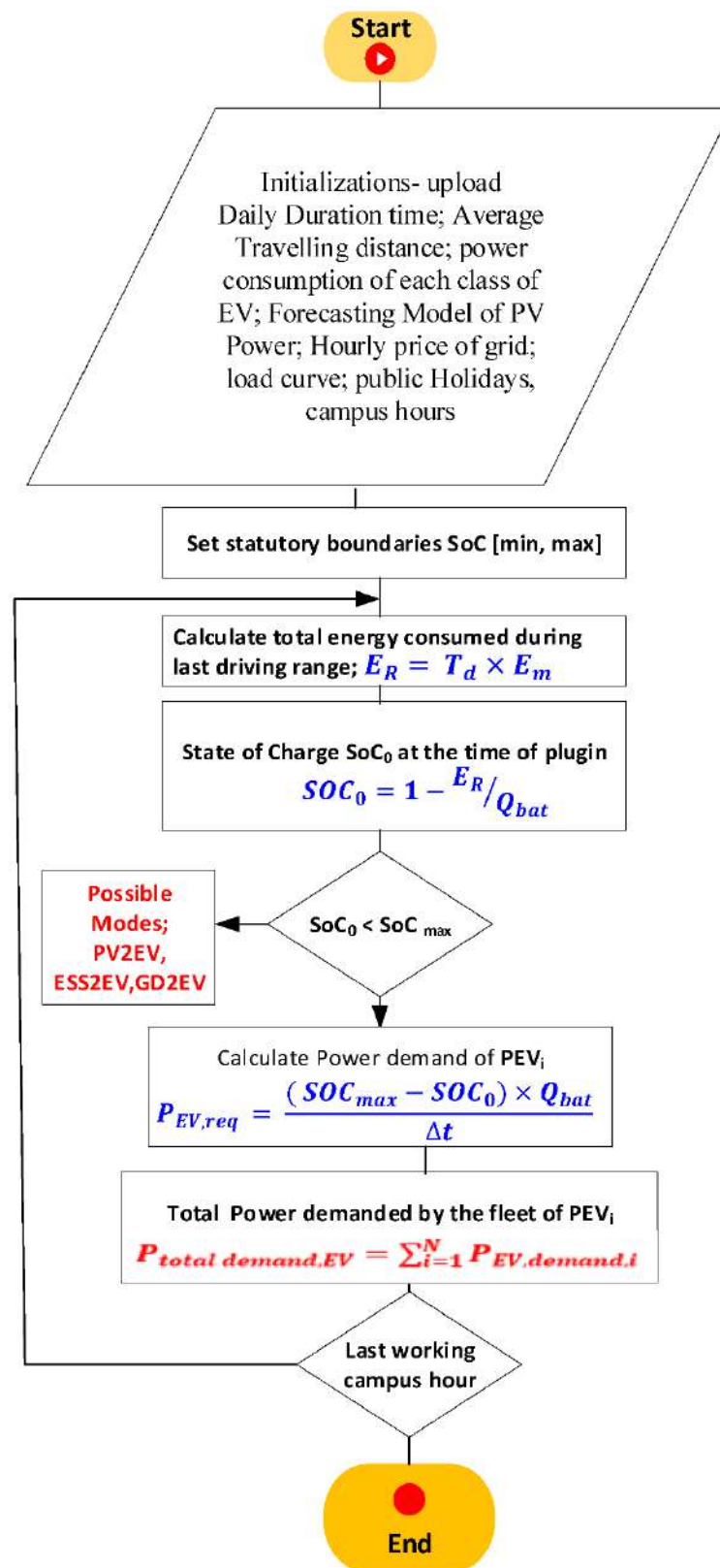

Figure 10. The flow path of the total demand of a fleet of electric vehicles.

3.2. Modes of Charging

Charging modes are linked in the way of power flow throughout the network. In each mode, the way of power drift is encountered to streamline the power demand and generation. To attain this goal, a set of predetermined voltage-current thresholds is needed to switch the modes as exhibited in [24]. The operating modes energize the energy influx among several entities of the charging station i.e., (PV array, ESS, grid, and EV) according to certain pre-defined rules.

Fast overlook of the completely proposed procedures incurred in the improvement of heuristic precedence REMA depicted in pictorial format as marked in Figure 11.
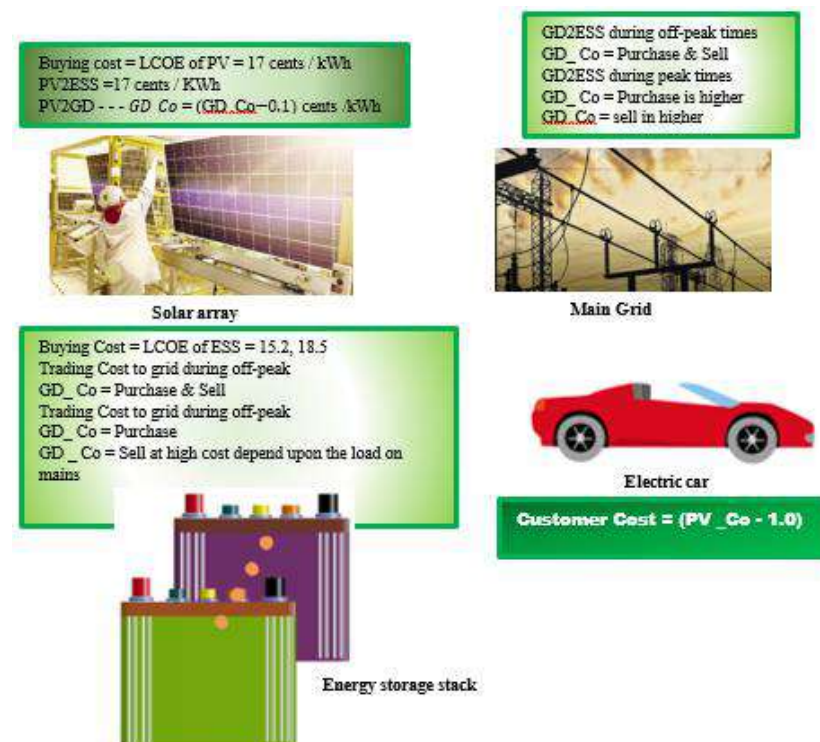

Figure 11. Pictorial view of energy trading among different entities.

3.3. Operation of the Transactive Grid with REMA under Variant Scenarios

The operating modes accelerate the energy flux among several entities of the charging station (solar-powered array, power storage variables, power grid, and vehicles) according to certain pre-defined rules. The working of the understudied system is explained in four different modes of operation depending on the solar irradiation conditions and SOC of the EV battery.

(i)   Overload: it executes when EV_{demand} is more than PV_{power}
(ii)   Under load: it executes when EV_{demand} is present but less than or equal to PV_{power}
(iii) No-load: it executes when the PV_{power} is available but the EV_{demand} is zero
(iv)   Idle condition: it executes when both EV_{demand} and PV_{power} is zero.

3.3.1. Overloaded Scenario

In this scenario when the solar panels extracting power, it directly charges the e-cars via converters instantly (PV2EV). As the condition for an overload scenario is $EV_{Dmd} > PV_{Pwr}$, the sole photovoltaic cannot fulfill the EV_{Dmd}; whilst the rest is satisfied by ESS or the public grid. If the main grid is at off-peak hours, the *GD2EV* is energized. Simultaneously, the SOC of the battery bank is rechecked; if *SOC* is less than *SOCM*, then the energy bank is also accumulated by the grid (*GD2ESS*) at low *GD_Co* (*Me_GD_Co* < *ESS_Co*). Henceforth, both vehicles and energy banks are taking advantage of low *GD_Co* by a valley-filling

operation. In contrast, if the grid is fully loaded and $Avl\_ESS\_Pwr > EV_{Dmd}$, the demand is realized by battery stacks exclusively using ESS2EV. However, if $Avl_{ESS_{Pwr}} <$ rest EV_{Dmd}, the grid aids the energy bank to supply power to vehicles (GD2EV). In an extreme case, if both renewable and standby have inadequate energy, the rest EV_{Dmd} is encountered by the grid GD2EV. It is worth citing that the energy is sold to staff vehicles at fixed Chg_Co regardless of the sources. Besides, no restriction is imposed on vehicle owners to participate in de-regulated markets without his will even in the overload scenario, hence enjoying autonomous charging. Figure 12 represents the operation flow path during an overloaded scenario.
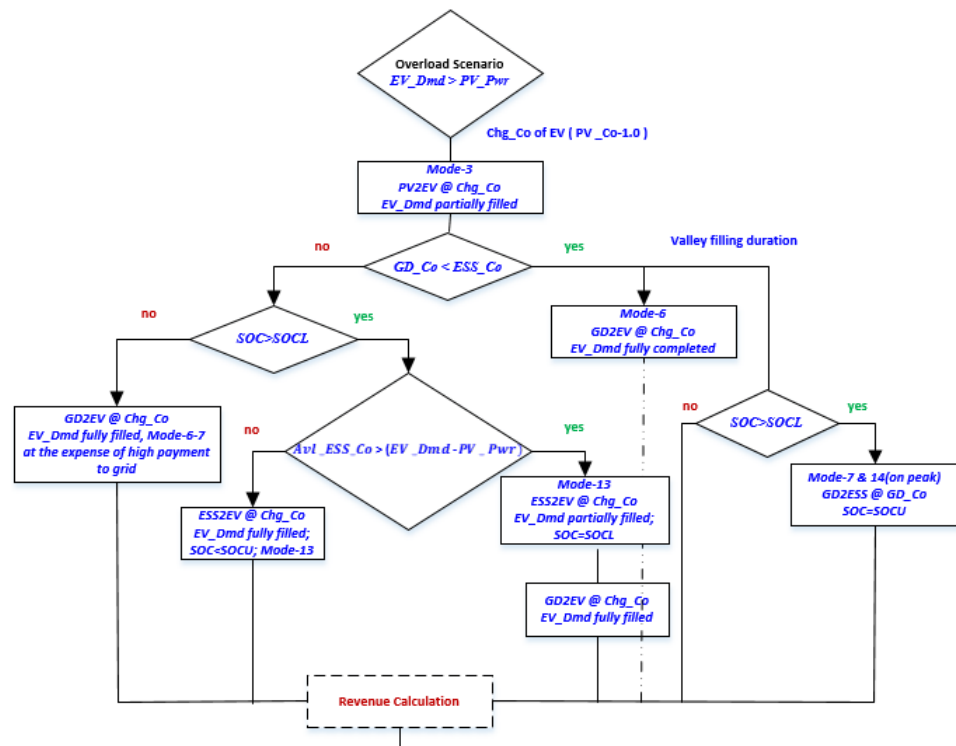

Figure 12. The flow path of the overload scenario.

3.3.2. Under Load Scenario

In this scenario, the empowered $PV\_Pwr > EV\_Dmd$; therefore, the extra PV_Pwr can be injected into ESS to raise its state charge. Otherwise, it may be traded to the public grid for monetary gain. The surplus PV_Pwr is given preference to accumulate ESS (PV2ESS). Though, if $Red\_ESS\_Pwr >$ extra PV_Pwr, the rest of the demand is compensated by a valley-filling option using mode GD2ESS. In contrast, if the additional $PV\_Pwr > Red\_ESS\_Pwr$, the residual energy is retailed to the utility grid (PV2GD). In case, if ESS is priorly fully saturated, then the whole additional PV_Pwr is transferred to the public grid. Figure 13 expresses the flow path during this scenario.

3.3.3. No Load Scenario

During load less test, the gross PV_Pwr has two options: (i) to recharge the ESS and/or (ii) to inject the public grid. The state charge of ESS is first monitored; in case the level is lower than the upper threshold, then PV_Pwr is employed to recharge the ESS (PV2ESS). Nevertheless, if the PV_Pwr supersedes *residual bank power* $\left(Red_{ESS_{Pwr}}\right)$, the spare power is shifted to the mains (PV2GD) choosing Mode-1. On the other hand, if $Red_{ESS_{Pwr}} > PV\_Pwr$, the ESS can extract the rest of power-extracted from upstream (GD2ESS) via valley-fill procedure. Conversely, in case the ESS approaches the upper threshold, the absolute PV_Pwr is translated to the mains (PV2GD). The flow path of the no-load scenario as shown in Figure 14.
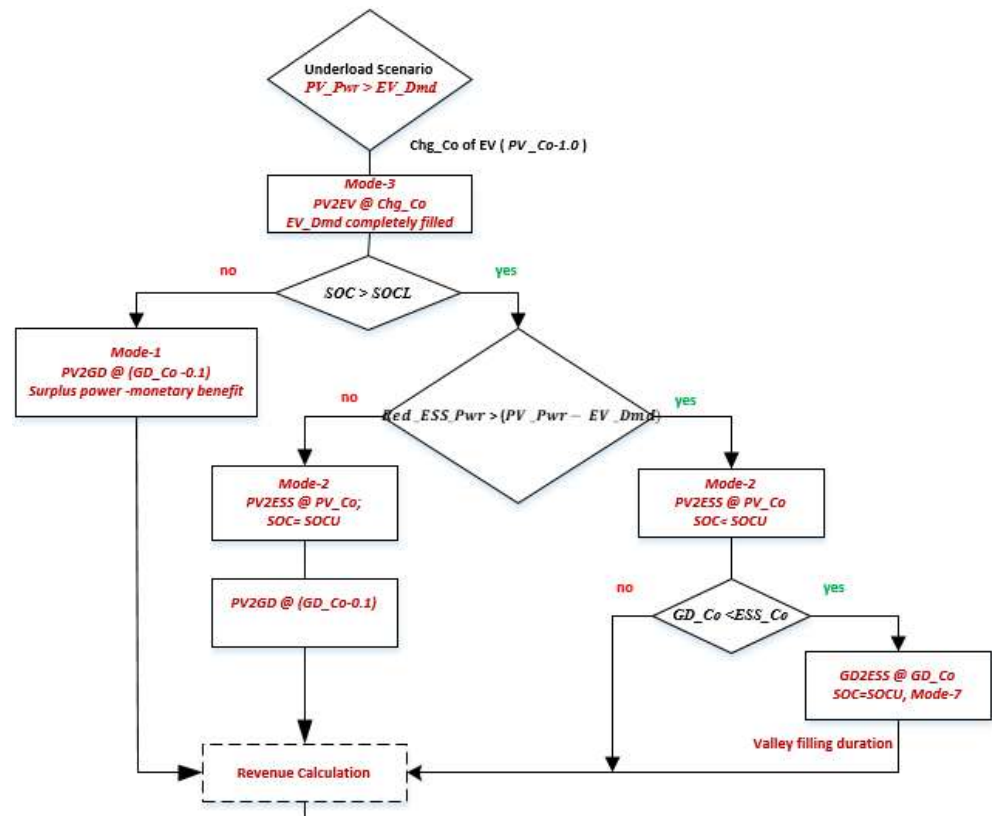
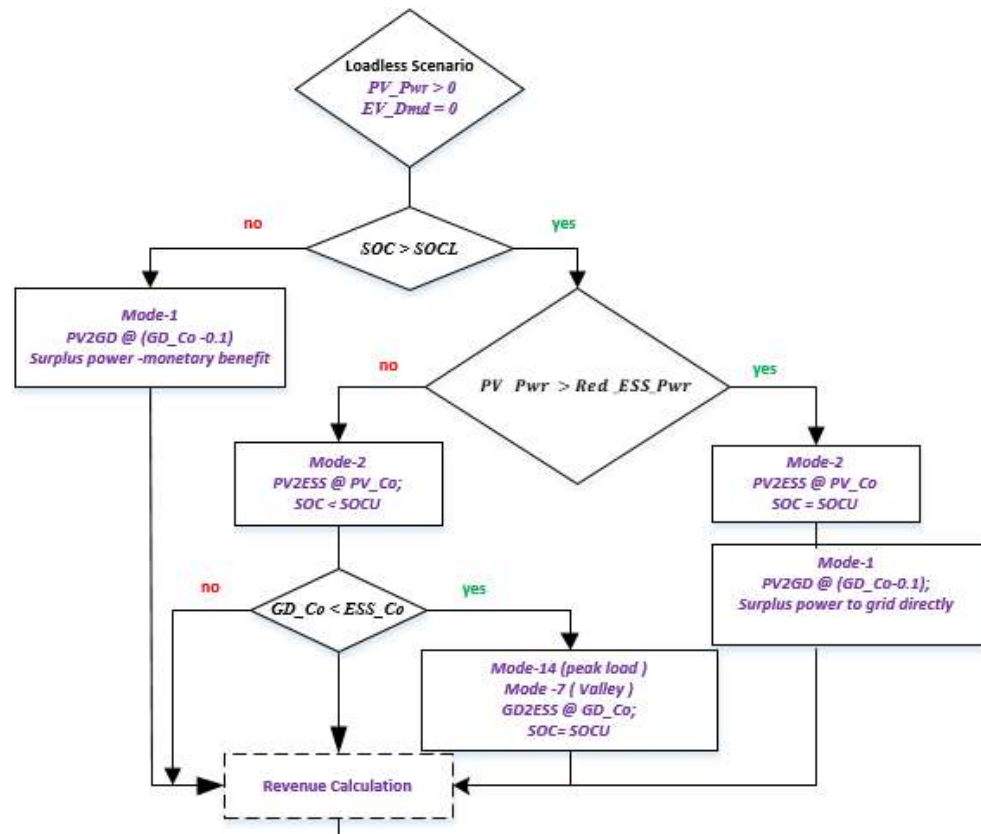**Figure 13.** Under load scenario of the fast charging dock station.

Figure 14. No-load test scenario of charging station.

3.3.4. Idle State Scenario

The recharging of ESS commences when the state charge is lower than the up-threshold and the mains are at the off-loaded condition. The combined procedure during the dead (idle) scenario is furnished through a unit operating course. This dead scenario exhibit a vital show in lessening the financial deficit of the recharging electric station. However, to enhance the lossless movement of the electric station while servicing a specified fleet of EVs, it is significant to explore the optimum size of solar arrays and battery bank units. In this p, the optimal sizes are computed by optimizing the business prototype model of the electric station. The precedence rule-based heuristic operation of the electric charging facility in this idle scenario is displayed in Figure 15.
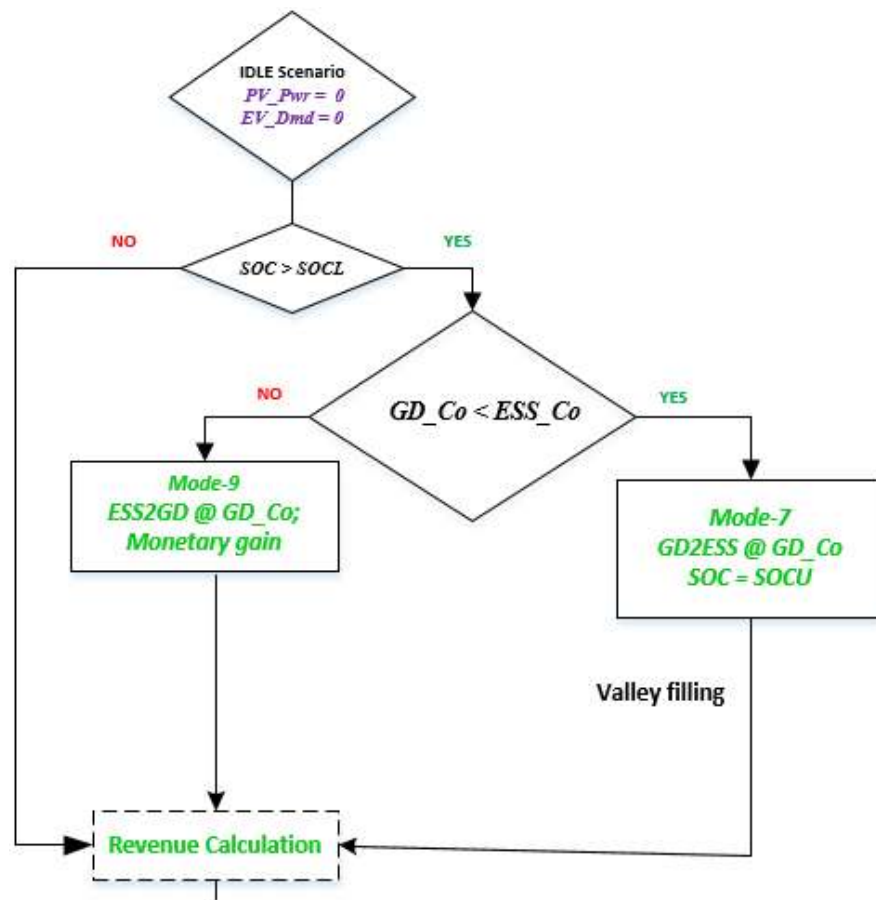

**Figure 15.** Idle test scenario of recharging port.

4. Confab and Discussion

The understudied intelligent charging dock is a prototype carport garage in a workspace, possibly an academic campus, which covers 1000 parking sides. It accepts that 15% of the 1000 cars stay every day except holidays in this recharging station, i.e., 150 cars are EVs while the rest are fossil-powered vehicles. These 150 EVs were selected as a test case targeted in this study. The variant car models are shown in tabular form in Table 2 [51] and the distribution of car models is shown in Figure 16.

Table 2. Parameters of variant sizes of electric vehicles. Adapted from [51].

EV Model	Commute Percent	Capacity Consumption	Energy Mileage
	%	kWh	kWh/miles
Sedan Delux	32	0.2	0.2
Full size Sedan Standard	38	0.3	0.3
Average (Mid) size SUV	20	0.45	0.45
Full size SUV	10	0.6	0.6
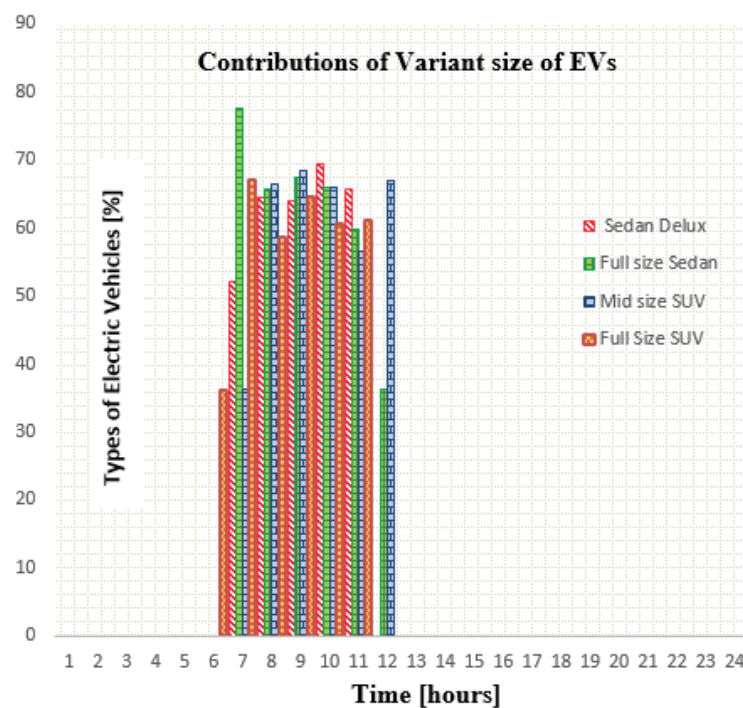
Figure 16. The current state of charge of EVs at arrival to electric station.

To facilitate a photovoltaic-grid EV rapid charging facility that assurances seamless daylight recharging at a fixed value (*PV_Co*—1.0 cents/kWh), the starting way is to define the optimum size of components of the recharging area to suppress yearly financial losses while attaining the targets of REMA. For the e-station size computation, the modeling equations, techno-economical parameters are used during the diligence of optimization methods. Furthermore, the optimization algorithm employs dynamic control schemes (REMA in this understudied paper) that express fitness functions and given constraints [52]. To optimum resize the charging deck, optimal number of PV modules (N_{pv}) and ESS stationary batteries (N_{bat}) for a specified number of EVs are extracted using the Harris Hawk Optimization (HHO) algorithm. The model of vehicles tested in this project are found in [53,54]. The percentage portion of individual electric vehicle, connected to the car station is framed in [19].

To ensure the resiliency of the shrewd REM algorithm under a variant number of occupied days, the network sizing is inhibited for various scenarios of non-occupied days and city general holidays for the whole year. In this study, resource optimization HHO was applied as a benchmark for four cases of holidays: (i) general holidays i.e., off campus days holidays with two weekends (H+2W), (ii) one weekend i.e., public holidays with one weekend (H+1W), (iii) null weekend and general holidays (H + 0W) and (iv) null holidays (0H+0W) i.e., 365 days per year.

4.1. Optimal Number of PV Arrays and Batteries in ESS

As the charging station is assumed to operate based on the optimal profit principle, N_{pv} and N_{bat} need to be correctly determined. Otherwise, the station may run into a loss. Since PV modules and batteries require high investment, the optimized combination of these two components is very important. Thus, to obtain the best combination, barebones Harris hawk optimization (HHO) is used to find N_{pv} and N_{bat} [55]. To validate the supremacy of HHO, compared with multifarious PSO and memetic GOA.

4.2. Cost Function and Constraints

The target of the barebones HHO is to search the best number of solar modules and ESS batteries that gratify the *EV_Dmd* while utilizing the grid energy with the least priority, such that the disparity between the trading and buying prices of energy (i.e., revenue) is minimum. However, the difference in prices should not be less than zero i.e.,$min\{Profit(n_p)\} \geq 0$, thus to evade the system's financial losses. Therefore, the profit minimization results in the optimal number of solar panels and batteries in the charging station. The selling and trading cost expressed in the following equations.

$$
\begin{aligned}
Selling\ Cost\ &\left(S_{eny}^t\right)\\
&= (PV2EV_{ET} + ESS2EV_{ET} + GD2EV_{ET}) \times (\ PV_{Co} - 1.0) + (PV2GD_{ET})_t \times (GD_{Co} - 0.1)\ + (PV2ESS_{ET})\\
&\times PV_{Co} + (GD2ESS_{ET}) \times (GD_{Co})_t
\end{aligned}
\tag{16}
$$

$$
\begin{aligned}
Buying\ Cost\ &\left(B_{eny}^t\right)\\
&= (PV2EV_{ET} + PV2ESS_{ET} + PV2GD_{ET})_t \times (\ PV_{Co}) + (ESS2EV_{ET})_t \times (ESS_{Co})\\
&+ (GD2EV_{ET} + GD2ESS_{ET}) \times (GD\_Co)_t
\end{aligned}
\tag{17}
$$

Applying this condition and values in Equations (16) and (17), the objective function J for the HHO is written as; S_{eny}^t and B_{eny}^t are energy buying and trading prices at interval t, respectively. By putting the values of S_{eny}^t and B_{eny}^t in Equation (18), the expanded cost function J is portrayed as;

$$
minimization \rightarrow J\left(n_p\right) = min\left(\frac{1}{100}\sum_{t=1}^{T}(S_{eny}^t - B_{eny}^t)\right)
\tag{18}
$$

where n_p is a set of decision variables. These decision variables include N_{pv} and N_{bat} whose minimum numbers are determined during the optimization process.

The number of solar modules and the battery should be integers and within the minimum and maximum limits [55].

$$
N_{pv} \rightarrow integer, \quad N_{pv}^{min} \leq N_{pv} \leq N_{pv}^{max}
\tag{19}
$$

Similarly, for the batteries stack

$$
N_{bat} \rightarrow integer, \quad N_{bat}^{min} \leq N_{bat} \leq N_{bat}^{max}
\tag{20}
$$

4.3. Discourse of Charging Station Sizing

The procedure described above for optimal system sizing was used under a different number of holidays. Additionally, the sizing is done for a specific number of vehicles to be recharged per day (150). The results are achieved by setting up the parameters of HHO as given in [55]. These parameters are listed in Table 3.

**Table 3.** Decision control parameters of HHO algorithm.

Decision Parameters	Notation
Position of Harris Hawk, Position of ith Harris Hawk	X, X_i
Prey best position	X_{rabbit}
Location of a random agent	X_{rand}
Mean position of swarm	X_{mean}
Number of eagles, iteration metrics, max set-bounds	N, t, T
Randomly value in range (0,1)	$r_1, r_2, r_3, r_4, r_5, q$
Dimensions, upper and lower bounds of decision variables	D, LB, UB
Escape Energy, Initial Escape Energy	E, E_0

Table 4 portrays the optimal number of battery units and solar modules to get optimal cost function by the HHO algorithm as a benchmark.

Table 4. Optimal profit using meta-heuristic algorithms.

Fleet of EVs	Optimization	N_{pv}	N_{bat}	Fitness Function @ Convergence
		$N_{pv}^{min} = 100, N_{pv}^{max} = 900, N_{bat}^{min} = 10, N_{bat}^{max} = 50$		
	HHO	765	43	0.02805
		763	44	0.04194
		760	42	0.00833
150	PSO	765	43	0.02198
		752	32	0.06610
	GOA	765	43	0.01591
		43	13	0.2438

The convergence curve of barebones HHO is simulated in Figure 17. Moreover when the HHO compares with the other AI based population based canonical PSO [56] and mimetic grasshopper optimization algorithms (GOA) for charging components sizing it ranks prominently. Figure 18 shows the supremacy of HHO with counterpart swarm algorithms.
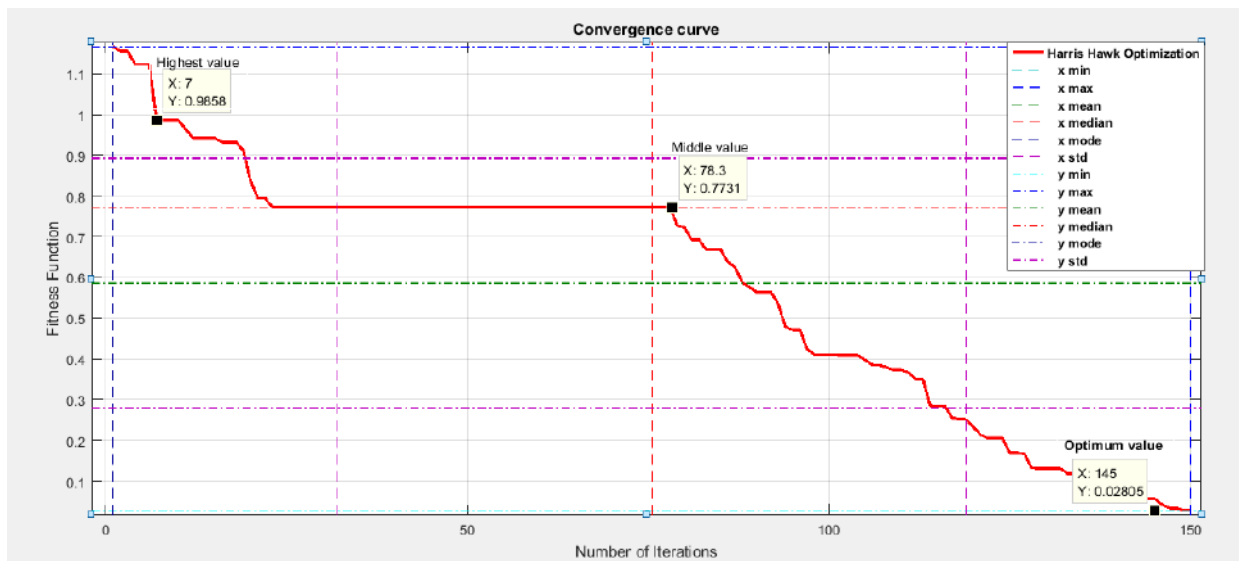
Figure 17. Outclass performance fitness function by barebones HHO.
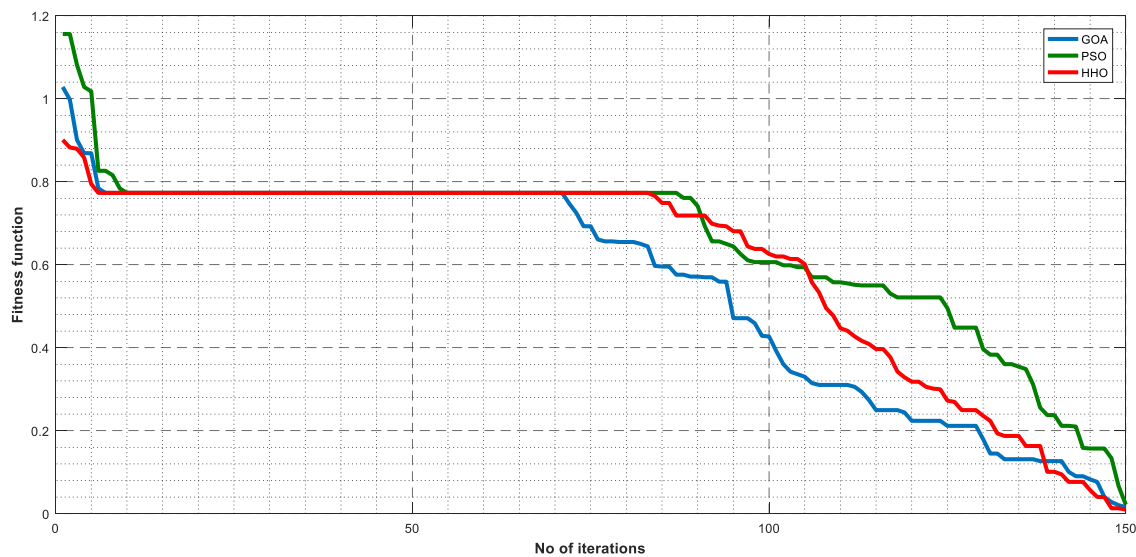
Figure 18. Comparative results of meta-heuristic algorithms of GOA, PSO, HHO.

The various conditions under which the system was tested for REMA resiliency were:

(a) Meteorological conditions (winter, summer, normal and abnormal days)
(b) Vocations (i.e., H + 2W, H + 1W, H + 0W, 0H + 0W)
(c) EV fleet size (for 150 EVs)
(d) Par and below parity states (PS, 0.83PS, 0.33PS)
(e) LCOE of ESS (15.2 cents/kWh, 18.5 cents/kWh)
(f) Operational periods of electric station (single day, 1 week, and 1 year)

4.4. Results under Diverse Climatic Conditions

The proposed shrewd energy management was validated with different seasonal times, normal and abnormal days, number of holidays, and parity states condition for its effectiveness and robustness.

4.4.1. Resiliency in Winter

Figure 19 depicts the recharging horizon of 150 EVs during an explicit winter single day at par parity state (PS), i.e., *PV_Co = Me_GD_Co*, as depicted from the subplot (iv). The generation of the *PV_Pwr* from solar in the subplot (i) was obvious—which shows that the insolation was not intervened by abrupt variation in climate such as heavy rain, snowfall, cloudy day, etc. During this particular normal day, the insolation was low so the *PV_Pwr* was inadequate to recharge all vehicles using PV2EV (PV energy to charge EV) operating mode. In this condition, the *EV_Dmd* was realized without charging intrusion by other sources, i.e., by activating additional modes, namely ESS2EV (ESS energy to charge EV), and GD2EV (grid energy to charge EV).

4.4.2. Resiliency in Summer

Figure 20 depicts the charging simulation results for a specific summer working day. For the same number of modules, it is to be noted that the PV produced more power compared to the winter day. Generally, the summer day was lengthy; photo arrays began to provide power before campus working timings and lasted to supply electricity beyond the campus hours. This can be noticed in the subplot (i). The surfeit *PV_Pwr* lessened the local grid dependency by evading the initiation of GD2EV as delineated by the subplot (ii). Additionally, the excess *PV_Pwr* compensated the system financial losses by selling the surplus energy to the grid using mode PV2GD, shown by the subplot (iii) with the blue dotted line "vending surplus energy to mains".
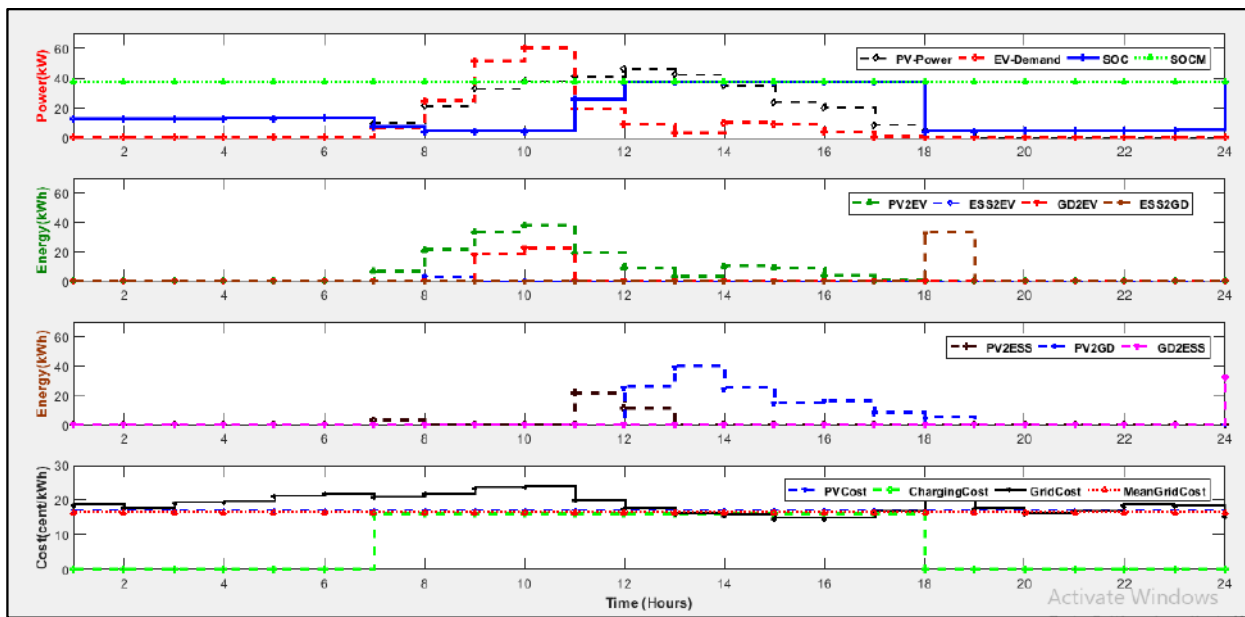
Figure 19. Precedence heuristic optimal power flow in winter day at PS.
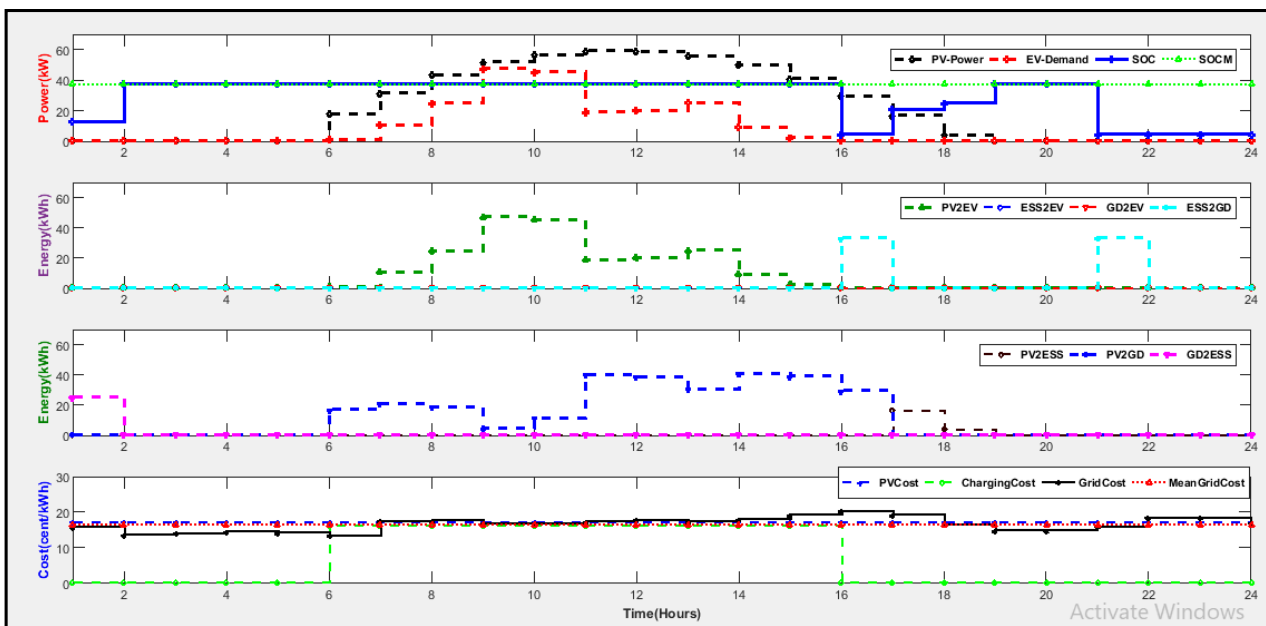

Figure 20. Precedence heuristic rule based energy utilization strategy in summer day at PS.

4.4.3. Resiliency in Abnormal Weather

Figure 21 depicts the working for a defined day (winter) with harsh climatic conditions i.e., the sporadic solar insolation. This intermittency imitated by fluctuated irradiance (*PV_Pwr*) during the entire day, as marked by the subplot (i). Nevertheless, it is clear from the subplot (i) that the *EV_Dmd* was satisfied without any disturbance, irrespective of fluctuations in *PV_Pwr* as well as in *EV_Dmd*. Furthermore, subplot (iv) depicts that recharging was performed with a fixed value regardless of incessant variations in *GD_Co*. It is important to note that this fixed price was also lower than *Me_GD_Co.*
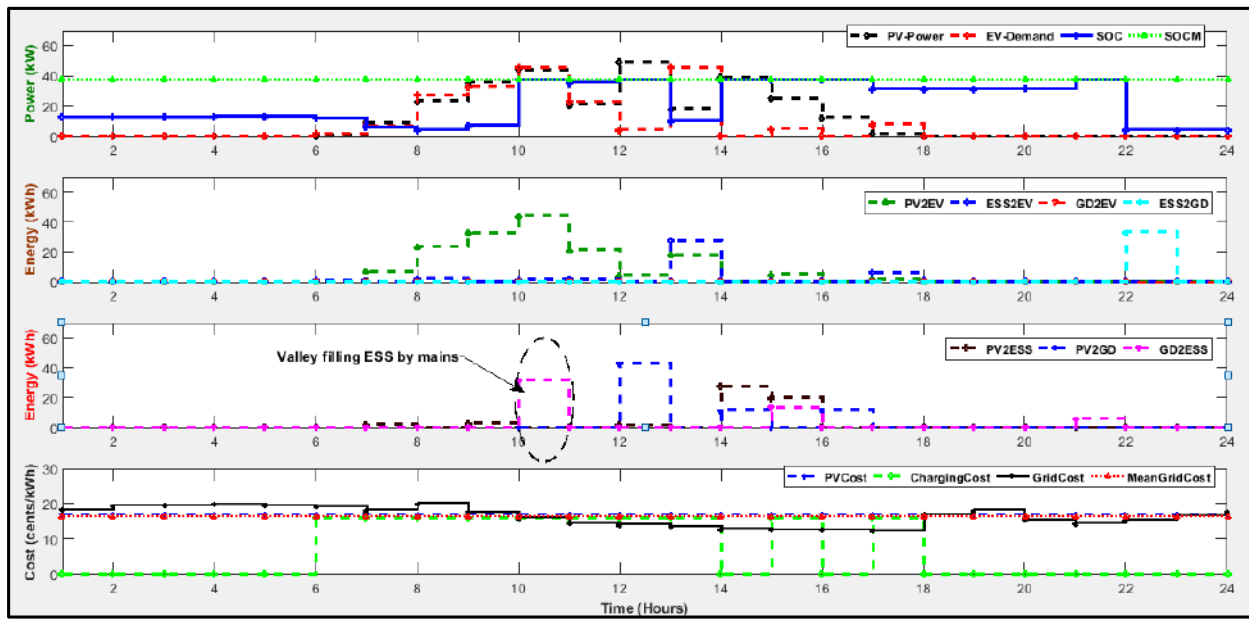
Figure 21. Precedence based energy reallocation scheme for thunderstorm single day.

4.4.4. Resiliency during Holiday

Figure 22 shows the operation for a specific holiday. Subplot (i) reveals the no-load scenario, where the *PV_Pwr* was available but there was no EV to be charged due to an office holiday. However, once the ESS reached the *SOCM* limit, it remained constant throughout the day as shown in the subplot (i). The valley-filling operation is shown in subplot (iii) during the hours 6 to 8 with label "Valley-filling status by ESS".

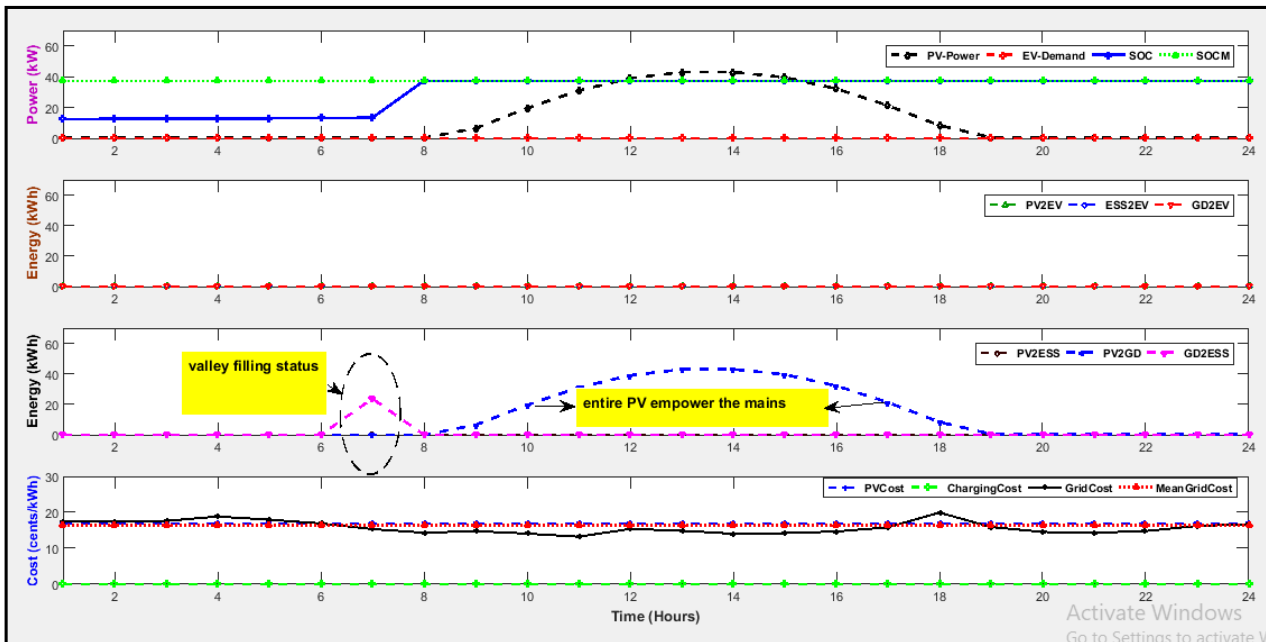

Figure 22. Rule-based energy-efficient scheduling during campus holidays at PS.

4.4.5. Resiliency under Different Parity States

The previous results are obtained when the charging station was operating at par parity state, i.e., *PV_Co = Me_GD_Co*. However, it can be proved that the REMA was resilient in providing constant and low-cost charging without intervention at low levels of

parity. Figure 23 presents the behavior of charging station for a specific day for 150 EVs per day at below parity, i.e., *PV_Co* was 0.83 times of *Me_GD_Co*. This condition is depicted in the subplot (iv) where *Me_GD_Co* was more than *PV_Co*.
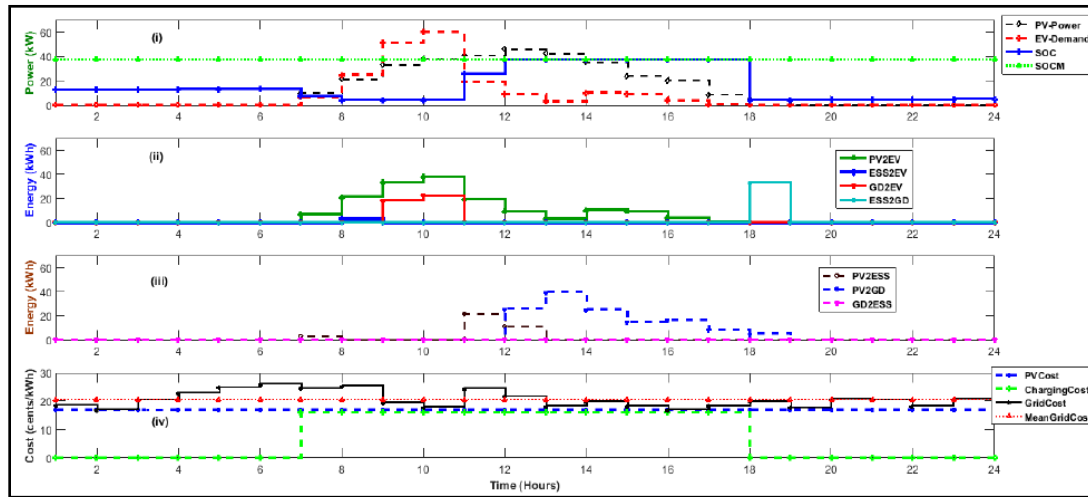

Figure 23. Mean Grid cost is 1.2 times than solar module cost for 150 EVs.

Since the results in Figure 23 were computed for the same winter day i.e., the charging profile was the same as in Figure 19. However, for the below parity there was a small shift of valley-filling operation by ESS, as shown in plot (iii). For the parity case, the valley-filling took place for only 1 hour, but for the lower parity, it was delayed by 1 hour. This is due to the increase of *GD_Co*. In the present case, the *GD_Co* fulfilled the condition of valley-filling (i.e., *GD_Co* < *ESS_Co*) during hours 9 to 11. It shows that with higher *GD_Co*, the valley-filling operation could be delayed or suspended. The suspension of flat valley filling by ESS.

Similarly, Figure 24 depicts the graphs once *PV_Co* was 0.33 times of *Me_GD_Co*.
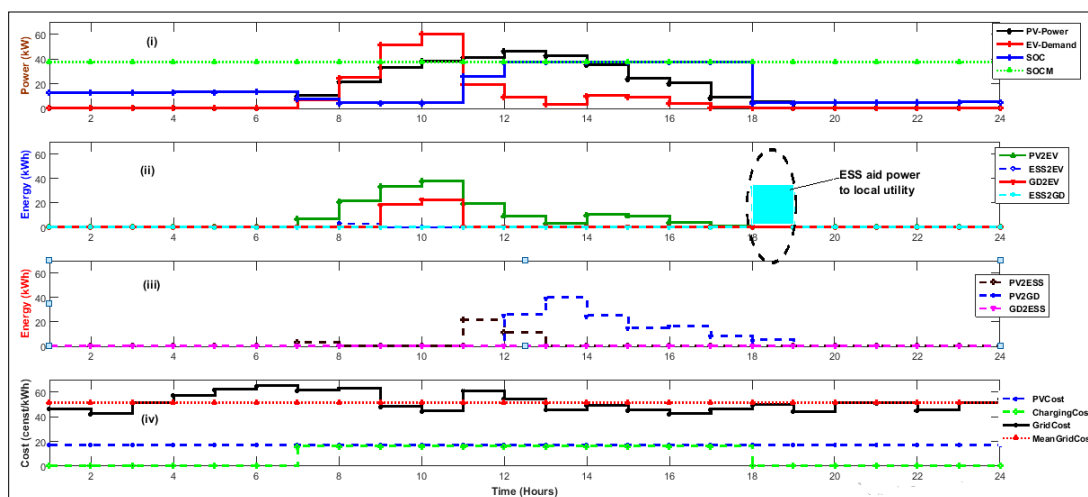
Figure 24. Mean Grid cost is triple than solar module cost for 150 EVs.

4.4.6. Resiliency in 1 Week

Figure 25 depicts the action of the electric station for one explicit week during the winter season. The 1-week duration includes all 7 days. It is evident from the graph that there were no vehicles charging demand in the weekend or public holiday. By taking advantage of these holidays, the charging station owner sold total PV energy solely to the

grid using GD2ESS. In addition, from the subplot (iii) that the flat valley time-division charging (GD2ESS) was executed in each working hour. Henceforth, during the diurnal of the specified days (particularly in the winter season when solar insolation was low), the storage stack energy was employed to sustain the seamless charging. Consequently, its state charge was lessened that triggers the valley-time filling process. Conversely, due to the sunny climate solar irradiance was quite adequate, the *PV_Pwr* was normally enough to satisfy the *EV_Dmd*. Hence the less utilization of the ESS, which marked a lesser number of valley-time filling processes in respect to winter seasons.
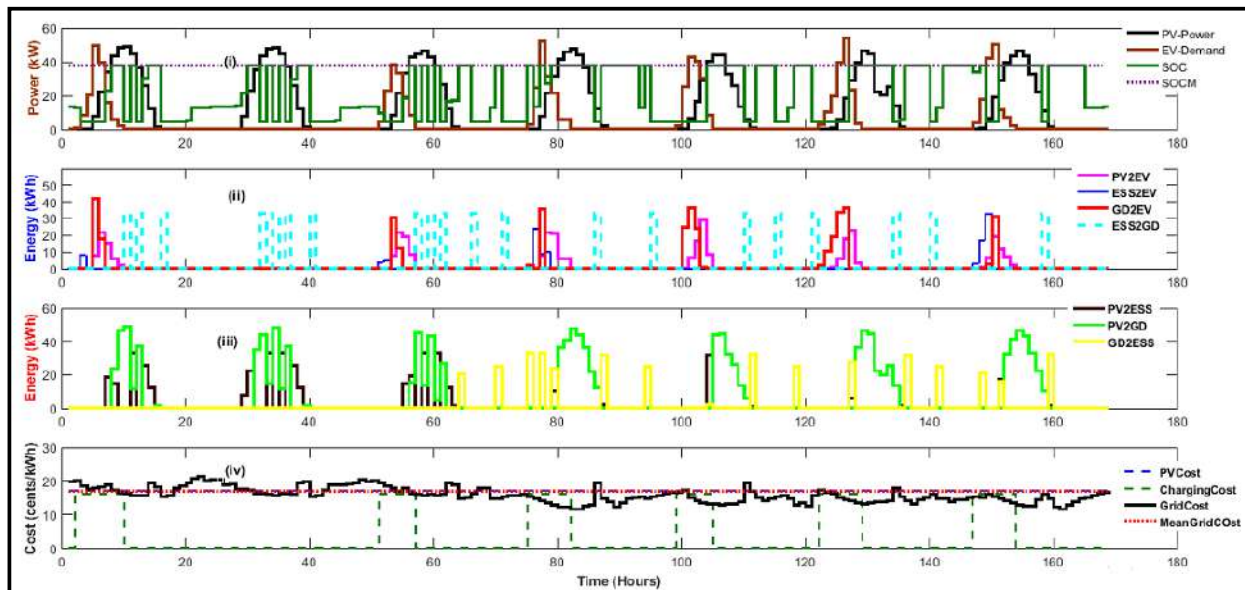

Figure 25. Week operation including one holiday in winter at parity using heuristic energy precedence.

4.4.7. Resiliency in 1 Year

Figure 26 depicts the action of the electric station for the whole year. The previously mention statements that were debated under unit day procedures can be noted from the results of the whole year. For instance, it is evident from the subplot (i) generated *PV_Pwr* (black color dotted lines) was upper in summer season rather than winter which displayed continuous varying nature during the whole year. Thus, as debated before, subplot (iii) shows that the amount of solar energy traded to the grid (PV2GD) was higher during summer as related to winter, which majorly compensateed for the station monetary losses in the winter season due to low insolation and fixed charge charging pattern.

To summarize the work of the paper, the main theme and value are given as;

Rule-based energy management algorithm (REMA) for the solar-grid tied EV rapid recharging system in the campus facility was applied to accelerate the operation of electric energy from the PV modules, storage tanks, and national grid that was established in the understudied research. The salient features of REMA were to facilitate the owners of EVs to recharge at a fixed cost lesser than mean grid electricity cost during operational periods. Additionally, utilizing the REMA algorithm the solar-grid recharging scheme could run disruption-less at a lower cost subject to PV grid parity was reached.

The rules were verified under various conditions of climate, different parity levels, LCOE of energy storage banks, zero-carbon vehicle fleet size and operational times. It was confirmed that the vehicle fleet demand was accomplished at a fixed price regardless of uncertainties of solar power, grid electricity costs, and vehicle power needs. Additionally, the charging station of definite size did not suffer any monetary loss even when operated at par and below parities.
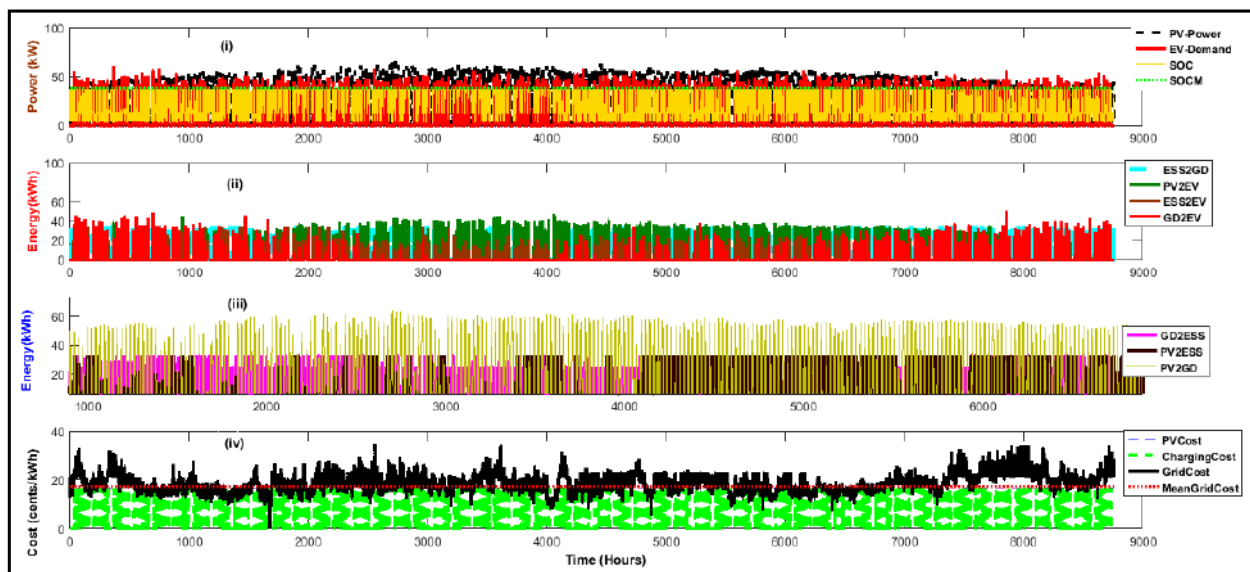
Figure 26. Annual operation at parity using heuristic optimal power scheme.

The proposed optimal sizing using SI based algorithm (HHO) for the grid-connected microgrid whilst employing the REMA algorithm (REMA-HHO) was also benchmarked with REMA-PSO and REMA-GOA. The supremacy of the devised REMA-HHO based approach for optimal sizing of the EV charging station was confirmed in terms of minimizing the objective function. The comparative evaluation of the algorithms showed that REMA-HHO yielded a better result as it offered the optimal profit at the US $ 0.0083/kWh, as compared to the REMA-PSO at the US $ 0.0661/kWh and REMA-GOA at the US $ 0.2438/kWh.

5. Conclusions

The understudied research has effectively developed and validated the proposed shrewd REMA to support the RES in delivering an un-disrupted EV charging at a constant value (which is smaller than the mainstream electricity cost). Simulation and experimental results were presented to prove the system's effectiveness under dynamic and various conditions. Although the rules defined in the energy utilization scheme marked in this paper explicitly devised for the particular case in hand, the approach is generic and thus can be a valuable path for practitioners, engineers, planners in building a coherent system in high dimension. This is vital because the deplore size of the photo modules and battery storage units are the main sources of optimal implementation of the hybrid solar-grid rapid charging infrastructure. The presented scheme dealt with the solar-powered EV charging place. For future work, an annex to the work can integrate with other renewable resources such as tidal, diesel, wind power, and biomass, etc. Moreover, the proposed supervisory REMA is applicable only for those geographical regions that have already achieved grid parity portfolio. The other challenging task is to reconsider systems that can work beyond the grid level parity (i.e., LCOE of PV modules above than mean grid electricity cost).

Author Contributions: Conceptualization, M.P.A.; Methodology, Z.A.A. and A.H.S.; Supervision, M.P.A. and U.U.S.; Validation, Z.A.A. and M.K.A.; Visualization, G.F. and H.S.H.; Writing—original draft, Z.A.A.; Writing—review and editing by M.A.K. All authors have read and agreed to the published version of the manuscript.

Institutional Review Board Statement: Not applicable.

Informed Consent Statement: Not applicable.

References

1. Boulanger, A.G.; Chu, A.C.; Maxx, S.; Waltz, D.L. Vehicle Electrification: Status and Issues. *Proc. IEEE* **2011**, *99*, 1116–1138. [CrossRef]
2. Elgowainy, A.; Han, J.; Poch, L.; Wang, M.; Vyas, A.; Mahalik, M.; Rousseau, A. *Well-To-Wheels Analysis of Energy Use and Greenhouse Gas Emissions of Plug-In Hybrid Electric Vehicles*; Argonne National Laboratory (ANL): Argonne, IL, USA, 2010.
3. Arfeen, Z.A.; Khairuddin, A.B.; Munir, A.; Azam, M.K.; Faisal, M.; Bin Arif, M.S. En route of electric vehicles with the vehicle to grid technique in distribution networks: Status and technological review. *Energy Storage* **2019**, *2*. [CrossRef]
4. Chian, T.; Wei, W.; Ze, E.; Ren, L.; Ping, Y.; Bakar, N.A.; Faizal, M.; Sivakumar, S. A Review on Recent Progress of Batteries for Electric Vehicles. *Int. J. Appl. Eng. Res.* **2019**, *14*, 4441–4461.
5. Arfeen, Z.A.; Abdullah, P.; Hassan, R.; Othman, B.M.; Siddique, A.; Rehman, A.U.; Sheikh, U.U. Energy storage usages: Engineering reactions, economic-technological values for electric vehicles—A technological outlook. *Int. Trans. Electr. Energy Syst.* **2020**, *30*, 12422. [CrossRef]
6. Tie, S.F.; Tan, C.W. A review of energy sources and energy management system in electric vehicles. *Renew. Sustain. Energy Rev.* **2013**, *20*, 82–102. [CrossRef]
7. Mahfouz, M.M.M.; Iravani, R. A Supervisory Control for Resilient Operation of the Battery-Enabled DC Fast Charging Station and the Grid. *IEEE Trans. Power Deliv.* **2021**, *36*, 2532–2541. [CrossRef]
8. Jiang, Z.; Rahimi-Eichi, H. Design, modeling and simulation of a green building energy system. In Proceedings of the 2009 IEEE Power & Energy Society General Meeting, Calgary, AB, Canada, 26–30 July 2009; pp. 1–7.
9. Betz, J.; Werner, D.; Lienkamp, M. Fleet Disposition Modeling to Maximize Utilization of Battery Electric Vehicles in Companies with On-Site Energy Generation. *Transp. Res. Procedia* **2016**, *19*, 241–257. [CrossRef]
10. El-Bayeh, C.Z.; Alzaareer, K.; Aldaoudeyeh, A.-M.I.; Brahmi, B.; Zellagui, M. Charging and Discharging Strategies of Electric Vehicles: A Survey. *World Electr. Veh. J.* **2021**, *12*, 11. [CrossRef]
11. Unger, R.; Schwan, T.; Mikoleit, B.; Bäker, B.; Kehrer, C.; Rodemann, T. "Green Building"—Modelling renewable building energy systems and electric mobility concepts using Modelica. In Proceedings of the 9th International MODELICA Conference, Munich, Germany, 3–5 September 2012; pp. 897–906. [CrossRef]
12. Lopez, J.E. Home charge system for EVs with peak power smoothing based on renewable energy. In Proceedings of the 2013 International Conference on New Concepts in Smart Cities: Fostering Public and Private Alliances (SmartMILE), Gijon, Spain, 11–13 December 2013; pp. 1–6.
13. Betz, J.; Hann, M.; Jager, B.; Lienkamp, M. Evaluation of the Potential of Integrating Battery Electric Vehicles into Commercial Companies on the Basis of Fleet Test Data. In Proceedings of the 2017 IEEE 85th Vehicular Technology Conference (VTC Spring), Sydney, Australia, 4–7 June 2017; pp. 1–7.
14. Betz, J.; Lienkamp, M. Approach for the development of a method for the integration of battery electric vehicles in commercial companies, including intelligent management systems. *Automot. Engine Technol.* **2016**, *1*, 107–117. [CrossRef]
15. Akhavan-Hejazi, H.; Mohsenian-Rad, H.; Nejat, A. Developing a Test Data Set for Electric Vehicle Applications in Smart Grid Research. In Proceedings of the 2014 IEEE 80th Vehicular Technology Conference (VTC2014-Fall), Vancouver, BC, Canada, 14–17 September 2014; pp. 1–6.
16. Mathur, A.K.; Yemula, P.K. *Scheduling of EV Charging in Grid-Connected Parking Lots with Renewable Sources*; Indian Institute of Technology: Hyderabad, India, 2018.
17. Arfeen, Z.A.; Sheikh, U.U.; Khalid, S.A.; Saeed, M.S.; Hafeez, F.; Faisal, M.; Ahmed, H.B. Energy Management Scheme for Electric Vehicles with Rapid-charging Facility Utilizing Grid Power Storage Packs and Photovoltaic Generator. In Proceedings of the 2020 IEEE International Conference on Automatic Control and Intelligent Systems (I2CACIS), Shah Alam, Malaysia, 20 June 2020; pp. 25–32.
18. Arfeen, Z.A.; Khairuddin, A.B.; Larik, R.M.; Saeed, M.S. Control of distributed generation systems for microgrid applications: A technological review. *Int. Trans. Electr. Energy Syst.* **2019**, *29*, 12072. [CrossRef]
19. Ma, T.; Mohammed, O.A. Optimal charging of plug-in electric vehicles for a car-park infrastructure. *IEEE Trans. Ind. Appl.* **2014**, *50*, 2323–2330. [CrossRef]
20. Mohamed, A.; Salehi, V.; Ma, T.; Mohammed, O. Real-Time Energy Management Algorithm for Plug-In Hybrid Electric Vehicle Charging Parks Involving Sustainable Energy. *IEEE Trans. Sustain. Energy* **2013**, *5*, 577–586. [CrossRef]
21. Wu, Y.; Zhang, J.; Ravey, A.; Chrenko, D.; Miraoui, A. Real-time energy management of photovoltaic-assisted electric vehicle charging station by markov decision process. *J. Power Sources* **2020**, *476*, 228504. [CrossRef]
22. Jiang, T.; Putrus, G.; Gao, Z.; Conti, M.; McDonald, S.; Lacey, G. Development of a decentralized smart charge controller for electric vehicles. *Int. J. Electr. Power Energy Syst.* **2014**, *61*, 355–370. [CrossRef]

23. Yong, J.Y.; Ramachandaramurthy, V.K.; Tan, K.M.; Mithulananthan, N. Bi-directional electric vehicle fast charging station with novel reactive power compensation for voltage regulation. *Int. J. Electr. Power Energy Syst.* **2015**, *64*, 300–310. [CrossRef]
24. Goli, P.; Shireen, W. PV powered smart charging station for PHEVs. *Renew. Energy* **2014**, *66*, 280–287. [CrossRef]
25. Preetham, G.; Shireen, W. Photovoltaic charging station for Plug-In Hybrid Electric Vehicles in a smart grid environment. In Proceedings of the 2012 IEEE PES Innovative Smart Grid Technologies (ISGT), Washington, DC, USA, 16–20 January 2012; pp. 1–8. [CrossRef]
26. Faruque, M.; Zhang, Y.; Dinavahi, V. Detailed Modeling of CIGRÉ HVDC Benchmark System Using PSCAD/EMTDC and PSB/SIMULINK. *IEEE Trans. Power Deliv.* **2005**, *21*, 378–387. [CrossRef]
27. Liu, Y.; Tang, Y.; Shi, J.; Shi, X.; Deng, J.; Gong, K. Application of Small-Sized SMES in an EV Charging Station with DC Bus and PV System. *IEEE Trans. Appl. Supercond.* **2014**, *25*, 1–6. [CrossRef]
28. Rahbari, O.; Vafaeipour, M.; Omar, N.; Rosen, M.A.; Hegazy, O.; Timmermans, J.-M.; Heibati, S.; Bossche, P.V.D. An optimal versatile control approach for plug-in electric vehicles to integrate renewable energy sources and smart grids. *Energy* **2017**, *134*, 1053–1067. [CrossRef]
29. Oliveira, D.; De Souza, A.Z.; Delboni, L. Optimal plug-in hybrid electric vehicles recharge in distribution power systems. *Electr. Power Syst. Res.* **2013**, *98*, 77–85. [CrossRef]
30. Arif, M.S.B.; Hasan, M.A. 2—Microgrid architecture, control, and operation. In *Hybrid-Renewable Energy Systems in Microgrids*; Fathima, A.H., Prabaharan, N., Palanisamy, K., Kalam, A., Mekhilef, S., Justo, J.J., Eds.; Woodhead Publishing: Sawston, UK, 2018; pp. 23–37.
31. Ayub, S.; Ayob, S.M.; Tan, C.W.; Ayub, L.; Bukar, A.L. Optimal residence energy management with time and device-based preferences using an enhanced binary grey wolf optimization algorithm. *Sustain. Energy Technol. Assess.* **2020**, *41*, 100798. [CrossRef]
32. Belfkira, R.; Zhang, L.; Barakat, G. Optimal sizing study of hybrid wind/PV/diesel power generation unit. *Sol. Energy* **2011**, *85*, 100–110. [CrossRef]
33. Zhang, W.; Ge, W.; Huang, M.; Jiang, J. Optimal Day-Time Charging Strategies for Electric Vehicles considering Photovoltaic Power System and Distribution Grid Constraints. *Math. Probl. Eng.* **2015**, *2015*, 1–9. [CrossRef]
34. Traube, J.; Lu, F.; Maksimović, D. Photovoltaic power system with integrated electric vehicle DC charger and enhanced grid support. In Proceedings of the 2012 15th International Power Electronics and Motion Control Conference (EPE/PEMC), Novi Sad, Serbia, 4–6 September 2012; pp. LS1d.5-1–LS1d.5-5.
35. Planas, E.; Andreu, J.; Gárate, J.I.; De Alegría, I.M.; Ibarra, E. AC and DC technology in microgrids: A review. *Renew. Sustain. Energy Rev.* **2015**, *43*, 726–749. [CrossRef]
36. Starke, M.; Tolbert, L.; Ozpineci, B. AC vs. DC distribution: A loss comparison. In Proceedings of the 2008 IEEE/PES Transmission and Distribution Conference and Exposition, Chicago, IL, USA, 21–24 April 2008; pp. 1–7.
37. Techakittiroj, K.; Wongpaibool, V. Co-existance between AC-Distribution and DC-Distribution: In the View of Appliances. In Proceedings of the 2009 Second International Conference on Computer and Electrical Engineering, Dubai, United Arab Emirates, 28–30 December 2009; Volume 1, pp. 421–425.
38. Ahmed, N.A. On-grid hybrid wind/photovoltaic/fuel cell energy system. In Proceedings of the 2012 10th International Power & Energy Conference (IPEC), Ho Chi Minh City, Vietnam, 12–14 December 2012; pp. 104–109.
39. Paul, A.; Subramanian, K.; Nachinarkiniyan, S. PV-based off-board electric vehicle battery charger using BIDC. *Turk. J. Electr. Eng. Comput. Sci.* **2019**, *27*, 2850–2865. [CrossRef]
40. Mukherji, A.; Subudhi, P.S.; Krithiga, S. Investigation of a PV Fed Improved Smart Home EV Battery Charging System using Multi Output Hybrid Converter. *Int. J. Renew. Energy Res.* **2019**, *9*, 692–703.
41. Eldeeb, H.; Faddel, S.; Mohammed, O.A. Multi-Objective Optimization Technique for the Operation of Grid tied PV Powered EV Charging Station. *Electr. Power Syst. Res.* **2018**, *164*, 201–211. [CrossRef]
42. Smaoui, M.; Abdelkafi, A.; Krichen, L. Sizing of a stand-alone hybrid system supplying a desalination unit. In Proceedings of the 2014 15th International Conference on Sciences and Techniques of Automatic Control and Computer Engineering (STA), Hammamet, Tunisia, 21–23 December 2014; pp. 820–824.
43. Chen, S.; Gooi, H.B.; Wang, M. Sizing of energy storage for microgrids. *IEEE Trans. Smart Grid* **2011**, *3*, 142–151. [CrossRef]
44. Saponara, S.; Saletti, R.; Mihet-Popa, L. Hybrid Micro-Grids Exploiting Renewables Sources, Battery Energy Storages, and Bi-Directional Converters. *Appl. Sci.* **2019**, *9*, 4973. [CrossRef]
45. Breyer, C.; Koskinen, O.; Blechinger, P. Profitable climate change mitigation: The case of greenhouse gas emission reduction benefits enabled by solar photovoltaic systems. *Renew. Sustain. Energy Rev.* **2015**, *49*, 610–628. [CrossRef]
46. Stuart, S.; Simon, H. *Redflow Investor Presentation*; Redflow: Brisbane, Australia, 2015.
47. Shao, S.; Jahanbakhsh, F.; Aguero, J.R.; Xu, L. Integration of pevs and PV-DG in power distribution systems using distributed energy storage Dynamic analyses. In Proceedings of the 2013 IEEE PES Innovative Smart Grid Technologies Conference (ISGT), Washington, DC, USA, 24–27 February 2013; pp. 1–6.
48. NREL Transforming Energy. Available online: https://www.nrel.gov/grid/solar-integration-data.html (accessed on 16 June 2020).
49. Gueye, S.; Belfkira, R.; Barakat, G.; Yassine, A. A Quadratic Model and A Heuristic for Sizing an Hybrid Renewable Energy System. In Proceedings of the Operational Research Practice in Africa (ORPA), Dakar, Senegal, 18–20 March 2010.

50. Shao, S.; Pipattanasomporn, M.; Rahman, S. Development of physical-based demand response-enabled residential load models. *IEEE Trans. Power Syst.* **2013**, *28*, 607–614. [CrossRef]

51. Ahmadian, A.; Mohammadi-Ivatloo, B.; Elkamel, A. A Review on Plug-in Electric Vehicles: Introduction, Current Status, and Load Modeling Techniques. *J. Mod. Power Syst. Clean Energy* **2020**, *8*, 412–425. [CrossRef]

52. Rawat, R.; Kaushik, S.; Lamba, R. A review on modeling, design methodology and size optimization of photovoltaic based water pumping, standalone and grid connected system. *Renew. Sustain. Energy Rev.* **2016**, *57*, 1506–1519. [CrossRef]

53. Zhang, L. Optimal Power Management of Parking-Lot Electric Vehicle Charging. Ph.D. Thesis, The University of Texas, Dallas, TX, USA, 2014.

54. Yilmaz, M.; Krein, P.T. Review of Battery Charger Topologies, Charging Power Levels, and Infrastructure for Plug-In Electric and Hybrid Vehicles. *IEEE Trans. Power Electron.* **2013**, *28*, 2151–2169. [CrossRef]

55. Maleki, A.; Ameri, M.; Keynia, F. Scrutiny of multifarious particle swarm optimization for finding the optimal size of a PV/wind/battery hybrid system. *Renew. Energy* **2015**, *80*, 552–563. [CrossRef]

56. Arfeen, Z.A.; Abdullah, P.; Shehzad, M.F.; Altbawi, S.; Jiskani, M.A.K.; Yiran, M.A.I. A Niche Particle Swarm Optimization-Perks and Perspectives. In Proceedings of the 2020 IEEE 10th International Conference on System Engineering and Technology (ICSET), Shah Alam, Malaysia, 9 November 2020; pp. 102–107.